

Review

Electromagnetic Irradiation Effects on MgO-based Magnetic Tunnel Junctions: A Review

Dereje Seifu ¹, Qing Peng ^{2,3,4,*}, Kit Sze ¹, Jie Hou ⁵, Fei Gao ⁶ and Yucheng Lan ^{1,*}

¹ Department of Physics and Engineering Physics, Morgan State University, Baltimore, MD 21251, USA

² Physics Department, King Fahd University of Petroleum and Minerals, Dhahran 31261, Saudi Arabia;

³ K. A. CARE Energy Research and Innovation Center at Dhahran, Dhahran, 31261, Saudi Arabia

⁴ Hydrogen and Energy Storage Center, King Fahd University of Petroleum and Minerals, Dhahran 31261, Saudi Arabia

⁵ School of Materials Science and Engineering, Georgia Institute of Technology, Atlanta, GA 30332, USA

⁶ Nuclear Engineering and Radiological Sciences, University of Michigan, Ann Arbor, MI 48109, USA

* Correspondence: qing.peng@kfupm.edu.sa (Q. P.); yucheng.lan@morgan.edu (Y. L.).

Abstract: Magnetic tunnel junctions (MTJs) have been widely utilized in sensitive sensors, magnetic memory, and logic gates due to their tunneling magnetoresistance. Moreover, these MTJ devices have promising potential for renewable energy generation and storage. Compared with Si-based devices, MTJs are more tolerant to electromagnetic irradiation. In this review, we summarize the functionalities of MgO-based MTJ devices under different electromagnetic irradiation environments, with a focus on gamma-ray irradiation. We explore the effects of these irradiation exposures on the MgO tunnel barriers, magnetic layers, and interfaces to understand the origin of their tolerance. The review enhances our knowledge of the irradiation tolerance of MgO-based MTJs, improves designs of these MgO-based MTJ devices with better tolerances, and provides information to minimize the risks of irradiation under various irradiation. This review starts with an introduction to MTJs and irradiation backgrounds, followed by fundamental properties of MTJ materials such as the MgO barrier and magnetic layers. Then, we review and discuss the MTJ materials and devices' irradiation tolerances under different irradiation environments, including high-energy cosmic radiation, gamma-ray radiation, and lower energy electromagnetic irradiation (X-ray irradiation, UV-Vis irradiation, infrared irradiation, microwave radiation, and radio-frequency electromagnetic irradiation). In conclusion, we summarize the irradiation effects based on the published literature, which might benefit material design and protection.

Citation: Seifu, D.; Peng, Q.; Sze, K.; Jou, J.; Gao, F. and Lan, Y. Irradiation Effects on MTJs. *Molecules* **2022**, *1*, 0. <https://doi.org/>

Received:

Accepted:

Published:

Publisher's Note: MDPI stays neutral with regard to jurisdictional claims in published maps and institutional affiliations.

Copyright: © 2023 by the authors. Submitted to *Molecules* for possible open access publication under the terms and conditions of the Creative Commons Attribution (CC BY) license (<https://creativecommons.org/licenses/by/4.0/>).

Contents

1. Introduction	2
1.1. Tunnel Magnetoresistance	2
1.2. Applications of MTJs	4
1.2.1. Electronics	4
1.2.2. Energy Harvesting	6
1.2.3. Energy Storage	7
1.3. Irradiation	7
1.3.1. Natural Radiation Sources	8
1.3.2. Artificial Radiation Sources	9
1.3.3. Radiation Units	10
1.4. Properties of MTJ Materials	10
1.4.1. Magnesium Oxide Barrier	10
1.4.2. Ferromagnetic Layers	10

1.5. Theoretic Irradiation Tolerance of MTJs	13	33
2. Effects of Cosmic Radiation	16	34
2.1. High-energy Heavy-Ion Irradiation	16	35
2.2. High-energy Proton Irradiation	17	36
2.3. High-energy Neutron Irradiation	18	37
2.4. High-energy Electron Irradiation	18	38
3. Effects of γ-ray Irradiation	18	39
3.1. MTJ Materials under γ -irradiation	20	40
3.1.1. MgO Crystals under γ -irradiation	20	41
3.1.2. Ferromagnetic Materials of MTJs under γ -irradiation	26	42
3.1.3. Interfaces of MgO Barrier / Ferromagnetic Layers	27	43
3.2. MTJs under γ -irradiation	27	44
3.2.1. Sensitive Results	27	45
3.2.2. Tolerant Results	27	46
3.3. Discussion on γ -irradiation of MTJs	31	47
3.3.1. γ -penetrations in MTJs	31	48
3.3.2. Possible Explanations of Radiation Degradation	31	49
3.3.3. Possible Explanations of Tunneling Tolerance	34	50
3.3.4. Possible Explanations for Divergence	35	51
4. Effects of Lower Energy Irradiation	36	52
4.1. X-ray Irradiation	36	53
4.2. UV-Vis Irradiation	36	54
4.3. Infrared Irradiation and Thermal Annealing	37	55
4.4. Microwave Irradiation	39	56
4.5. Radio Frequency Electromagnetic Irradiation	39	57
5. Outlook	39	58
6. Conclusions	40	59
References	41	60

1. Introduction

1.1. Tunnel Magnetoresistance

The phenomenon of tunnel magnetoresistance (TMR) has gained enormous attention in decades because of its essential applications in non-volatile magnetoresistive random-access memories (RAM) and next-generation magnetic field sensors [1–8]. This interest follows the emergence and success of related magnetoresistance such as anisotropic magnetoresistance (AMR) and giant magnetoresistance (GMR). Tunneling, as a foundational principle of TMR, arises from the quantum mechanical wave nature of particles and the non-zero probability of particles occupying classical forbidden regions.

The phenomenon of magnetoresistance (MR) was first discovered in 1856 [9] in nickel and iron sheets when subjected to parallel or perpendicular magnetic fields, which is known as anisotropic magnetoresistance (AMR). The magnitude of electric resistance changed about 2 % at room temperature for alloy AMR materials [10]. The AMR effect was attributed as a consequence of a higher probability of $s - d$ scattering of electrons traveling along the direction of magnetic fields [11]. Since the 1970s, the AMR effect has been utilized for magnetic recording.

Subsequently, a significant resistance variation, up to 50 %, was discovered in a sandwich metallic magnetic Fe / Cr / Fe multi-layers at room temperatures in the late 1980s [12,13], known as giant magnetoresistance (GMR). GMR was characterized as the

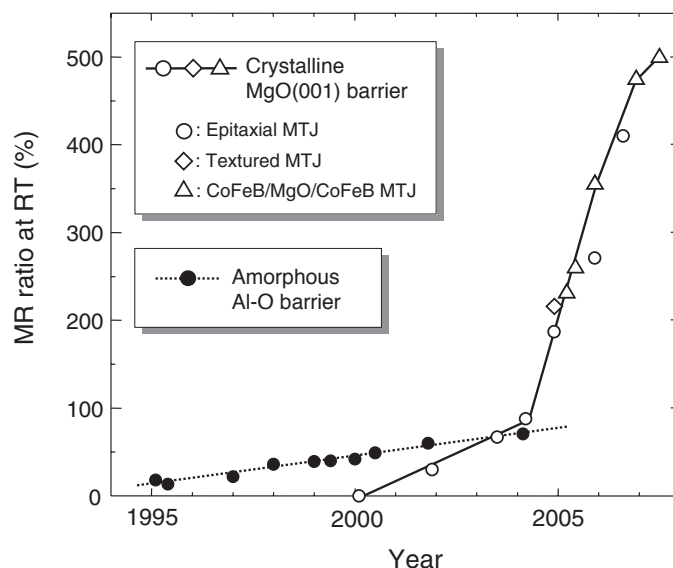


Figure 1. Historical development of MR ratio ratio of MgO-based MTJs at room temperature. The data of Al-O based MTJs were also plotted for comparison. Reproduced with permission [15]. Copyright 2008, the Physical Society of Japan.

difference in electrical resistance between parallel magnetic states (R_P) and anti-parallel magnetic states (R_{AP}) normalized by the parallel resistance R_P :

$$MR = \frac{R_{AP} - R_P}{R_P} \quad (1)$$

The GMR effect has been attributed to the spin-dependent scattering occurring at interfaces [14]. Presently, GMR is being widely utilized in modern hard drives as replacement for AMR devices for reading data.

Tunnel magnetoresistance (TMR) can be considered an extension of giant magnetoresistance (GMR) due to their similarities in electrical resistance changes of magnetic multilayer structures by aligning the magnetic moments of adjacent layers. Different from GMR, TMR employs a thin insulating layer as a tunneling barrier between magnetic layers, resulting in quantum mechanical electron tunneling across the barrier with a few nanometers in thickness. This leads to more significant changes in electrical resistance compared to GMR devices.

TMR technology and devices emerged in the 1990s as superior alternative to AMR and GMR devices for data storage due to their outstanding MR characteristics. Magnetic tunnel junctions (MTJs) are the core component of TMR devices. The development of MTJs was comprehensively reviewed recently [15–17]. Interested readers are encouraged to read the literature cited therein. Briefly, the tunnelling magnetoresistance (TMR) effect, which is explained by spin-polarized tunneling electrons, was first observed in Fe/Ge-O/Co multilayers in 1975 with an MR ratio of 14 % at 4.2 K [18]. In 1994, amorphous aluminum oxide (Al_2O_3) was introduced as a tunneling barrier material, achieving MR ratios of 18 % in Fe / Al_2O_3 / Fe layers [19] and 70 % in CoFeB / Al_2O_3 / CoFeB structures [20,21] in the 2000s. AlO_x -based MTJs have been reviewed recently and interested readers are referred to literature listed therein [22]. MgO-based MTJs were first investigated in the 1990s [23]. A moderate TMR of 20 % was achieved at room temperature in amorphous MgO-based MTJs. Crystalline MgO was later utilized as a tunneling barrier material, resulting in room temperature MR ratios of 30 % [5], 67 % [24], 88 % [25], 180 % [2], and 220 % [26] in crystalline Fe(001) / MgO(001) / Fe(001) MTJs, 230 % [3] and 355 % [27] in CoFeB / MgO / CoFeB MTJs, 410 % in Co(001) / MgO(001) / Co(001) MTJs [28], 500 % [15,16,29] and 604 % [30] in CoFeB / MgO / CoFeB MTJs. The highest MR ratio, 1,144 %, was observed at 4.2 K

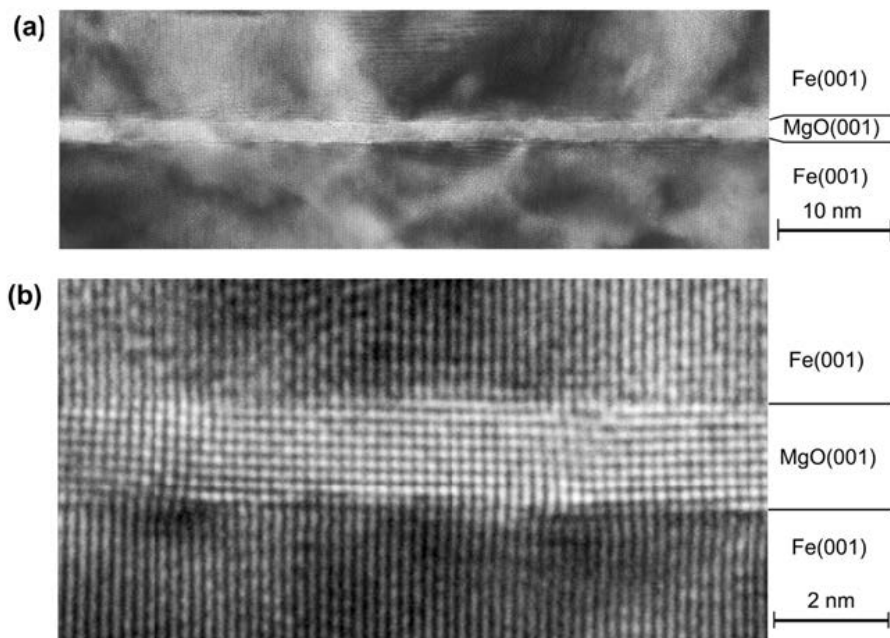


Figure 2. (a) TEM and (b) HRTEM images of a Fe(001) / MgO(001) / Fe(001) MTJ. Reproduced with permission [2]. Copyright 2004, Springer Nature.

in CoFeB / MgO / CoFeB MTJs [31]. The MR ratios of MgO-based MTJs have increased by over 50 times in less than two decades since the initial report, with some reviews of giant TMR in MgO-based MTJs published [15,32]. The history of MR ratios of both AlO_x -based and MgO-based MTJs is plotted in Figure 1. Clarifying the irradiation tolerance of these devices will lead to a deeper understanding of the physics of spin-dependent tunneling states.

MTJs consist of two ferromagnetic layers separated by a very thin insulator with a nanometer-scale thickness, typically made of amorphous Al_3O_3 or crystalline MgO. Figure 2 shows a typical MTJ consisted of a MgO crystalline barrier and Fe layers. Electrons tunnel across the insulating nanolayer from one ferromagnetic layer to the other, thereby contributing to the junction's electric conduction. The resistance of an MTJ is dependent on the relative magnetic alignment, either parallel or anti-parallel, of its ferromagnetic layers and its thin insulating layer.

Various ferromagnetic materials, including Fe, Co, FeCo alloys, and FeCoB, have been employed as MTJ ferromagnetic layers. Typically, these layers are crystalline in nature, with a specific orientation, such as Fe(001), chosen to match the crystalline barrier and increase MR ratios.

1.2. Applications of MTJs

MTJs have a broad range of applications in electronics, sensing, energy generation, and energy storage owing to their unique tunneling properties. A brief overview of these applications is presented below. Since the MR of MgO-based MTJs is significantly higher than that of AlO_x -based MTJs, our focus will only be on MgO-based MTJs here.

1.2.1. Electronics

One of the most known applications of MTJs is their use in data storage, particularly in MTJ-based memory devices [17,33–35], including dynamic random-access memory, flash memories, and hard disk drives. Data can be stored without the need for external magnetic fields [36]. Many review articles have been published on this topic, as listed in

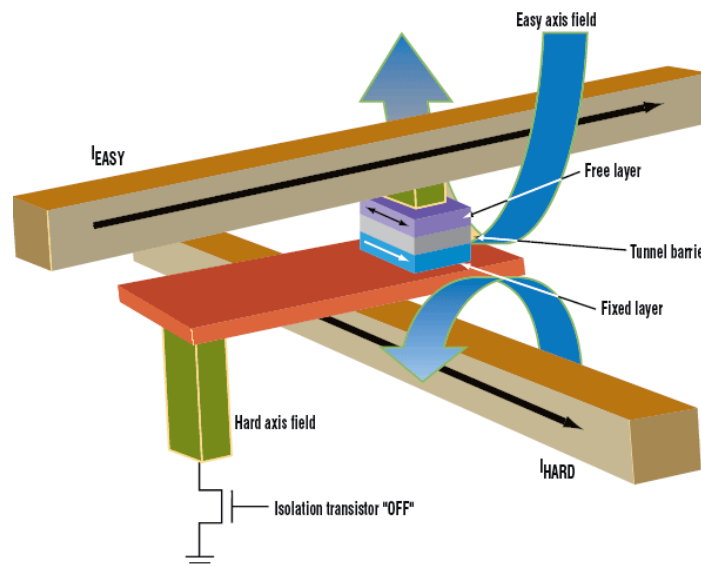


Figure 3. Structure of an MRAM cell (Courtesy of Freescale).

the preceding section. MgO-based TMJs exhibit high MR ratios at room temperature and have been utilized in hard disk drives (HDD) with high-density [17,34,37–41].

Additionally, a MTJ is comprised of two distinct states, namely, parallel and anti-parallel. Consequently, a single MTJ has the capability to store data in four different states [42]. Therefore, stacked MTJs are suitable for use in magnetic random-access memory (MRAM) applications [32] [2,7,17,43–51]. These nonvolatile MRAMs demand high MR ratios of > 150 % at room temperature.

Figure 3 shows a typical structure of an MRAM element. The element's primary component is an MTJ, which comprises a ferromagnetic free layer, an insulating tunnel barrier, and a ferromagnetic fixed layer. These sandwiched layers exhibit TMRs as a result of spin-dependent electron tunneling [32,43,44,52]. A recent review of the structure of MRAMs can be found in reference [50].

MRAM has the potential to replace all existing memory devices because of its capability of combining the speed of static random-access memory (SRAM) speed and the density of dynamic random-access memory (DRAM), while also being non-volatile like hard disk drives (HDD). Therefore, MRAM is a kind of highly desirable form of memory [16,20,33]. As a result, MTJ-based MRAM devices have been extensively investigated in the past two decades.

Compared with other kinds of random-access memory, MTJ-based MRAMs are a type of non-volatile memories that can work in irradiation environments, such as in outer space applications [53]. Irradiation tolerance of these MRAMs is critical to their effectiveness in such harsh environments.

In addition, MTJs have the potential to be employed as magneto-electric spin logic devices, which are capable of converting analog signals to digital ones. Various designs of analog-to-digital converters (ADCs) have been proposed [54–56], including Sigma-Delta ($\Sigma - \Delta$) ADCs with high bit-resolution [56]. As compared to traditional ADCs, the energy consumption of these MTJ-based ADCs is super low, down to 66 fJ for 4-bit MTJ-based ADCs and 37 fJ for 3-bit MTJ-based ADCs [55].

MTJ devices also have significant potential for sensing, such as ultra-sensitive magnetic field sensors [57,58], microwave frequency sensors [59], microwave power sensors [60], thermal sensors [61], and heat sensors [62].

1.2.2. Energy Harvesting

In addition to their conventional applications in memory and sensors, MTJ devices hold promise for renewable energy generation and storage. While relatively new in the field, MTJ-based energy devices have attracted considerable research attention. Although their device efficiencies are lower than these traditional energy devices, novel heterostructures of MTJs have the great potential to significantly impact the area. Lots of research groups have explored the fundamentals and future prospects of energy applications involving the spin of electrons. Various kinds of energy, ranging from heat and light to mechanical vibrations, have been successfully converted to electricity through spin conversion [35,62,63].

Heat:

Based on EU data, a considerable amount of industrial energy consumption ranging from 20 % to 50 % is lost as waste heat. In the United States, up to 1,734 trillion Btu of waste heat went unrecovered in 2008 [64]. The Seebeck effect, which involves a electromotive force (emf) generation under a temperature gradient, has been widely investigated in the past decades. Thermoelectric (TE) devices have the capability to harvest heat to electricity based on the Seebeck effect. Because of unique characteristics, such as no moving parts, quiet operation, low environmental impact, and high reliability, TE devices have attracted widespread interest since its discovery. In the past decades, semiconductor TE materials, especially ceramic nanocomposite bulks [65–69], have been developed for the purpose. Up to now, various TE nanocomposites have been investigated in absence of magnetic fields [70–81]. Device efficiency of up to 10 % can be achieved using the semiconductor TE devices.

Spin-caloritronics, the combination of spintronics and thermoelectrics, is an emerging field [62,82]. Electron spin waves interact with heat in insulating ferromagnets under magnetic fields through the magneto-Seebeck effects, also referred as the spin Seebeck effect or magneto-thermopower effects. A thermal gradient can lead to the production of magneto thermopower and magneto thermocurrent [83]. Therefore, spin caloritronic devices can serve as waste heat recyclers and heat sensors under magnetic fields.

MTJs devices, comprised of insulating barriers and ferromagnetic layers, can utilize spin-caloritronics to generate pure spin currents via magnetization dynamics induced by a temperature gradient. These MTJ devices have unique potential in harvesting thermal energy and there are many research focusing on MTJ-based heat recycling in the past decade. The spin-Seebeck coefficients of various MTJs have been measured under magnetic fields [82–88]. For examples, CoFeB / MgO / CoFeB MTJs have been integrated with resistance thermometers to recycle waste heat from spin Seebeck effect [62]. A Seebeck coefficient of Al₂O₃-based MTJs was measured up to 1 mV/K [89]. A large spin-dependent Seebeck coefficient of 100 μ V/K was observed in CoFeB / MgO / CoFeB MTJs [90]. However, due to their nanoscale thickness, the output power of MTJs is much lower than that of semiconductor TE bulk counterparts (up to kW). It was reported that a output TE power of a CoFeB / MgO / CoFeB MTJ device was only 10 pW per 12.6 cm² (\sim 10 nW/m²) [91]. Even compared with that of semiconductor TE film devices (up to several hundred W / m²), the output power is super lower for the state-of-art MTJ devices. Although the power output of present MTJ devices is unsatisfactorily low for industrial heat recyclers, MTJ devices are one kind of emerging energy-harvesting devices.

Solar energy:

In addition to their capacity of heat recycling, MTJs can generate electricity through the utilization of solar energy. Phonon can couple to the electron spin and magnon, which enables the generation of spin currents from solar energy [35]. More recently, photoinduced spin currents were observed recently [63]. Furthermore, the potential of MTJs was explored for spin photovoltaic applications [92].

Mechanical energy:

Recently, a new research field, known as spinmechanics or spinmechatronics, has emerged to combine spin currents with mechanical motion [63]. Spin currents can be generated from mechanical energy such as vibrations and sounds. [93,94]

In one word, MTJs have the capacity to convert different kinds of energy into electricity through the amalgamation of electron spin with established energy conversion techniques. These research areas are relatively nascent and are expected to possess great applications in the forthcoming decades.

Electromagnetic energy:

It was reported that MgO-base MTJs could produce significant DC voltage when exposed to microwave radiations [95]. A DC voltage was generated under microwave irradiation with frequency of 1 MHz to 40 GHz and power density of $10 - 10 \times 10^6$ mW/m², with a sensitivity of up to 5,000 mV/mW. Similar phenomena was also observed in AlO_x-based MTJs exposed to microwave with power of 1 – 100 mW and 1.5 – 2.5 GHz [59].

1.2.3. Energy Storage

MTJs have potential applications in the field of energy storage as well, particular with respect to batteries and capacitors, which are two kinds of popular devices to store energy. Recent work of MTJ-based energy storage devices are highlighted below.

Capacitors:

Magnetic capacitances of MTJs was first investigated in Co / Al₂O₃ / Co MTJs in the 2000s and their potential application is explored as supercapacitors for energy storage [96]. The tunneling magnetocapacitance (TMC) of Co₄₀Fe₄₀B₂₀ / MgO / Co₄₀Fe₄₀B₂ MTJs was measured at room temperature about two decades late [97,98]. The voltage-induced TMC ratio reached 1000 % due to the emergence of spin capacitance. An inverse of TMC was observed in Fe / AlO_x / Fe₃O₄ MTJs [99]. The inverse TMC reached up to 11.4 % at room temperature and could potentially reach 150 %. It is believed that the spin accumulation in anti-parallel configurations of MTJs leads to a difference in spin-up and spin-down diffusion lengths, creating a charge dipole that acts as an extra serial capacitance and gives rise to the observed TMC effect [100].

In a recent study, it was reported that MgO-based (001)-textured MTJs exhibited a significant TMC of 332 % at room temperature [101]. Subsequently, an even higher TMC of over 420 % at room temperature was achieved through using epitaxial MTJs with MgAl₂O₄ (001) barriers possessing a cation-disordered spinel structure [101].

These findings implicate potentials of MTJs for the development of capacitors and related technologies.

Batteries:

MTJ devices have also been employed as spin batteries for conversions of the magnetic energy of superparamagnetic nanomagnets into electricity [102]. The examined MTJs contained MnAs nanomagnets with a zinc-blende-structure. These nanomagnets were chargeable under magnetic fields, proving evidence for the existence of spin batteries. The resulting electromotive force (*emf*) was found to operate on a timescale of approximately $10^2 - 10^3$ seconds. The *emf* should result from the conversion of the magnetic energy of the super-paramagnetic nanomagnets into electrical energy during their magnetic quantum tunnelling.

MTJ devices have diverse applications, such as data storage, sensors, energy generation and storage, even under irradiation. Consequently, it is crucial to evaluate their capacity to withstand irradiation. Here we focus on the irradiation tolerance of MgO-based MTJs. The information would provide valuable insights into their stability, and benefit error-free operation and protection of MgO-based MTJ devices in irradiation environment.

1.3. Irradiation

MgO-based MTJs may work in various irradiation environments. Therefore, it is necessary to review both natural and artificial sources of irradiation prior to reviewing the irradiation tolerance of MoO-based MTJs.

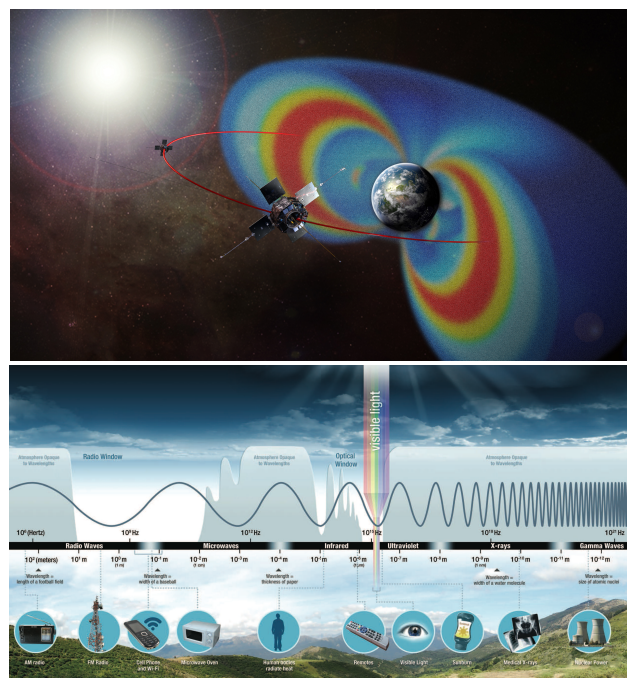


Figure 4. Radiation (a) in outer space and (b) on Earth. Satellites are orbiting in the radiation zone of the Van Allen belts whose cross-sectional shape and intensity are shown in (a). From nasa.gov.

1.3.1. Natural Radiation Sources

The Sun is the major natural radiation source in our life [103,104]. Nuclear fusion processes within the Sun produce cosmic rays that consist of high-energy atomic nuclei and electromagnetic waves, which spread through the solar system. These *primary cosmic rays* are composed primarily of 99 % nuclei (protons accounting for 90 %, alpha particles accounting for 9 %, and heavier element nuclei making up 1 %) and approximate 1 % solitary electrons and electromagnetic component (gamma-ray, X-ray, UV-visible light, and IR light). The energy of the primary cosmic rays is high up to 10^{20} eV. Owing to the Earth's magnetic field, the energetic particles are deflected and trapped within the Van Allen radiation belts. The belts extend from an altitude of about 640 km to 58,000 km above the Earth's surface, as shown in Figure 4a. The primary cosmic rays in the the Van Allen belts can expose various spacecraft components, including MTJ devices.

Upon entering the Earth's atmosphere, the primary cosmic rays collide with atoms and molecules present in the atmospheric layers [105]. These collisions produce *secondary cosmic particles* with lower energy and *electromagnetic waves*. The secondary particles and electromagnetic waves including low-energy neutrons, protons, electrons, alpha particles, γ -rays, and X-rays. The energy of the secondary cosmic particles and electromagnetic waves is much lower than those of the primary cosmic rays, but while still considerable. For instance, the energy of the secondary γ -rays can be 50 MeV on the Earth. Due to their sufficiently high energy, these secondary cosmic particles and electromagnetic waves can potentially damage MTJ devices, leading to soft errors in MTJ-based electronic integrated circuits.

There are natural radioactive minerals on the Earth, such as compounds containing uranium-238 (U-238) and thorium-232 (Th-232) radionuclides. These radioactive elements emit high-energy particles or rays in the natural environment. As such, these minerals are another kind of natural irradiation sources on the Earth.

Figure 4b shows the full spectrum of electromagnetic irradiation on the Earth. Table 1 lists the wavelength, frequency, and energy of various electromagnetic waves.

Thus, it is necessary to investigate potential radiation effects on microelectronic devices that exposed in outer space or on Earth. This is particularly important in the case of MTJ

Table 1. Properties of irradiation types.

Name	Wavelength	Frequency	Energy
cosmic radiation			up to 10^{20} eV
γ -ray	< 0.01 nm	> 30 EHHz	> 124 keV
X-ray	0.01 nm - 10 nm	30 EHHz - 30 PHz	124.8 eV - 124.8 keV
UV	10 nm - 400 nm	750 THz - 30 PHz	3.12 eV - 124.8 eV
visible	400 nm - 700 nm	430 THz - 750 THz	1.872 eV - 3.12 eV
infrared	700 nm - 1 mm	300 GHz - 430 THz	1.248 meV - 1.872 eV
microwave	1 mm - 0.1 m	3 GHz - 300 GHz	1.248 μ eV - 1.248 meV
radio	> 1 m	< 3 GHz	< 1.248 μ eV

KHz: 10^3 Hz; MHz: 10^6 Hz; GHz: 10^9 Hz; THz: 10^{12} Hz; PHz: 10^{15} Hz; EHz: 10^{18} Hz.

From Ref. [106] and nasa.gov.

Table 2. Some typical irradiation sources used in research laboratories.

Sources	Type	Energy	Ref.
cyclotron	heavy ions	10 MeV	[112,113]
EBIT	heavy ions	tens keV	[113,114]
Tandem accelerator	particles	20 - 40 MeV	[113,115]
FIB	gallium ions	30 keV	[113]
Nuclear reactor	neutron	500 MeV	[116]
TEM	electrons	80 - 200 keV	[117]
SEM	electrons	5 keV - 50 keV	[113]
^{24}Na source	γ -ray	2.76 MeV, 1.38 MeV	[118,119]
^{40}K source	γ -ray	1.46 MeV, 1.31 MeV	
^{60}Co source	γ -ray	1.33 MeV, 1.17 MeV	[120,121]
^{137}Cs source	γ -ray	0.66 MeV	[122]

TEM: transmission electron microscope; EBIT: electron beam ion trap facility; FIB: focused ion beam.

devices that are deployed in spacecraft, satellites, and airplanes, which operate in irradiation environment filling with high-energy particles and high-energy electromagnetic waves.

1.3.2. Artificial Radiation Sources

Besides the natural radiation sources, various artificial sources of radiation exist on the Earth, including nuclear weapons, nuclear power plants, television transmitting towers, microwave ovens, wireless phones. These artificial irradiation is also omnipresent in our surroundings, as shown in Figure 4b. For instance, modern microwave ovens used in kitchens can produce microwaves with a frequency of 2,450 MHz [107]. Cellphone towers can emit electromagnetic radiations with 800 MHz and 1900 MHz for 3G cellphone communications [108,109], with frequencies of 24 - 47 GHz for high-band 5G phones [109,110]. Moreover, even the human bodies can emit infrared radiation [111]. Although the energy of these artificial radiations is significantly lower than those of cosmic rays, it is still required to know if these artificial radiations damage MTJ devices or degrade MTJ device performances. Therefore, this review paper comprehensively examines radiation impacts of various electromagnetic waves, including γ -ray, X-ray, UV-visible light, microwaves, and even infrared radiation.

To date, various artificial radiation sources have been utilized in laboratories to quantitatively investigate irradiation effects on MgO-based MTJ devices. Most of the data reviewed here were collected on these radiation source. Table 2 lists some typical irradiation sources utilized in the cited literature here.

These artificial radiation sources can produce controllable electromagnetic particles in laboratories. Particle accelerators and synchrotron radiations, for instance, can generate high-energy particles, including neutrons and electrons, with energy ranging from 0.1 MeV to 1.0 MeV and high flux. γ -ray is usually generated from radioisotopes in laboratories, with energy from several keV to MeV. Some specialized devices, such as electron microscopes, can produce middle-energy particles with 5 – 200 keV. Commercial X-ray tubes can emit low-energy X-ray with tens of electronvolts. Various light sources, such as Xenon and halogen bulbs, can generate UV-visible light with energies in the electronvolt ranges. Additionally, infrared irradiation below 1 eV can be generated from electric furnaces in laboratories.

1.3.3. Radiation Units

The impacts of radiation are generally categorized into three types [104,105,123]: (1) Total Ionizing Dose (TID), which is quantified in Rad or Gray units. TID effects can change the threshold voltages of electronic devices due to trapping of charges during irradiation exposure. TID may cause leakages of electric currents. (2) Single Event Effects (SEE), which is not cumulative but results from individual interaction. SEE may cause soft errors and hard errors of devices. (3) Displacement Damage Dose (DDD), which can generate lattice defects. Sufficient displacement may change the device or material performance properties over time. TID and SEE are examples of ionizing radiation effects, while DDD is an instance of non-ionizing radiation effects. TID and DDD can lead to lasting damage to electronics over an extended period, showing long-term effects, whereas SEE typically results in immediate short-term effects. However, both short-term and long-term effects can potentially have permanent consequences.

To facilitate comprehension of the impact units, a brief summary is provided here. There are four kinds of ionizing radiation quantities: (1) Activity quantity, with units in becquerel (Bq), curie (Ci), and rutherford (Rd); (2) Exposure quantity, with units in coulomb per kilogram (C/kg) and röntgen (R); (3) Absorbed dose quantity, with units in gray (Gy), erg per gram, and radiation absorbed dos (Rad); and (4) Equivalent dose quantity, with units in sievert (Sv), röntgen equivalent man (rem). The definitions of these radiation quantities are also listed in Table 3 for readers without radiation background.

1.4. Properties of MTJ Materials

MgO-based MTJs are composed of MgO insulating barriers and ferromagnetic layers. The ferromagnetic layers consist of free-layers and fixed-layers, typically made of ferromagnetic Fe and CoFeB. In order to understand the irradiation tolerance of MgO-based MTJs, the physical properties of MgO and Fe / COFeB are first summarized below. The irradiation tolerance of MgO-based MTJs are related to these properties.

1.4.1. Magnesium Oxide Barrier

Magnesium oxide (MgO) possesses an ionic bonding structure, compositing of Mg²⁺ and O²⁻, with a crystallographic structure of rock salt (NaCl). Figure 5 shows its crystallographic structure. Figure 6 shows its monolayer structure. Magnesium and oxygen atoms alternately stack in the lattice.

MgO is an excellent electrical insulator, exhibiting a conductivity of 10⁻¹⁴ μ S/m at room temperature. Additionally, it is a soft magnetic material, with a magnetic susceptibility of -10.2×10^{-6} cm³/mol. The compound is also a refractory material, with physical and chemical stability up to 2500 °C. Its physical properties are listed in Table 4.

1.4.2. Ferromagnetic Layers

Ferromagnetic materials are utilized as free-/fixed layers in MgO-based MTJs. Crystalline (001) iron films were initially used as free-/fixed layers in MgO-based MTJs to achieve an MR ratio of 220 % [26,125] at the begin of the 2000s. Subsequently, crystalline

Table 3. Radiation unit and Terms.

Category	Unit	Definition
Activity	becquerel (Bq) *	activity of a quantity of radioactive material in which one nucleus decays per second (1/s)
	curie (Ci)	quantity or mass of radium emanation in equilibrium with one gram of radium (element), 1 Ci = 3.7×10^{10} Bq
	rutherford (Rd)	activity of a quantity of radioactive material in which one million nuclei decay per second, 1 Rd = 1,000,000 Bq
Exposure	röntgen (R)	quantity of radiation which liberates by ionization one esu (3.33564×10^{10} C) of electricity per cm ³ of air under normal conditions of temperature and pressure, 1 R = 2.58×10^{-4} C/kg
Absorption	Gray (Gy) *	dose of one joule of energy absorbed per kilogram of matter, 1 Gy = 1 J/kg = 100 rad = 10000 erg/gram
	radiation absorbed dose (Rad)	dose causing 100 ergs of energy to be absorbed by one gram of matter. 1 Rad = 0.01 Gy = 100 erg/gram
absorption	sievert (Sv) *	equivalent biological effect of the deposit of a joule of radiation energy in a kilogram of human tissue, 1 Sv = 1 J/kg = 100 rem
	roentgen equivalent man (rem)	unit of health effect of ionizing radiation. 1 rem = 0.010 Sv = 100 erg/gram
Dose		quantity of radiation or energy absorbed
Dose rate		dose delivered per unit of time
Exposure		amount of ionization produced by radiation. The unit is the roentgen (R).

*: SI unit. From epa.gov and nih.gov

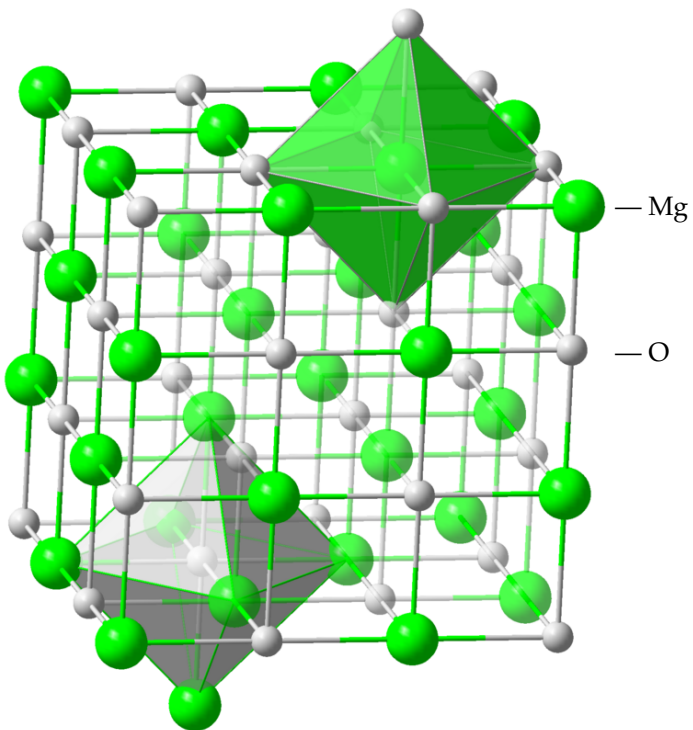


Figure 5. Crystallographic structure of MgO.

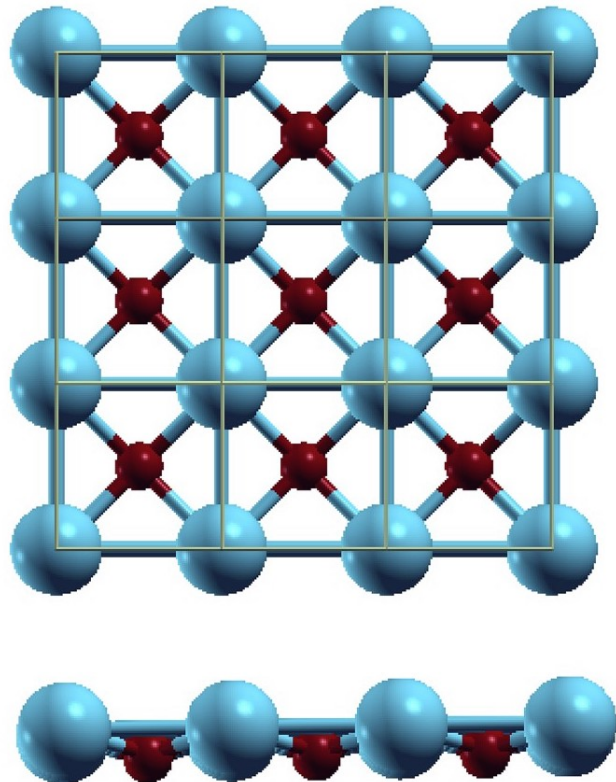


Figure 6. (a) Top view (along $<001>$ direction) and (b) side view (along $<100>$ direction) of a MgO (001) monolayer.

Table 4. Bulk properties of magnesium oxide (MgO) used as barrier layers in MgO-based MTJs [106].

Chemical formula	MgO
Space group	Fm $\bar{3}$ m, No. 225
Lattice constant	$a = 4.212 \text{ \AA}$
Cleavage	<100>
Molar mass	40.3044 g/mol
Coordination geometry	Octahedral (Mg^{2+}) and octahedral (O^{2-})
Density	3.58 g/cm ³ (25 °C)
solubility in water	0.0062 g/L (0 °C), 0.086 g/L (30 °C)
Melting point	2,852 °C (3,125 K)
Boiling point	3,600 °C (3,870 K)
Thermal conductivity	45 – 60 W/m/K (25 °C)
Thermal expansion	$138 \times 10^{-7} / ^\circ\text{C}$ (25 °C)
Heat capacity (C)	37.2 J/mol/K (24 °C)
Std molar entropy (S_{298}°)	26.95 J/mol/K
Std enthalpy of formation ($\Delta_f H_{298}^\circ$)	601.6 kJ/mol
Gibbs free energy ($\Delta_f G_{298}^\circ$)	-569.3 kJ/mol
Electrical conductivity	$10^{-14} \mu\text{S}/\text{m}$ (24 °C)
Band gap	7.8 eV [124]
Refractive index (n_D)	1.7355 ($\lambda = 0.633 \mu\text{m}$) 1.72 ($\lambda = 1 \mu\text{m}$)
Transparency	> 92 % ($\lambda = 0.25 – 7 \mu\text{m}$)
Thermal stability	up to 700 K
Dielectric constant	9.65
Magnetic susceptibility (χ)	$-10.2 \times 10^{-6} \text{ cm}^3/\text{mol}$

Co(001) films were employed as free-/fixed layers of MgO-based MTJs, achieving an MR ratio of 410 % [28]. Currently, CoFeB is extensively used in MgO-based MTJs, and the MR ratio has been enhanced to 500 – 600 % at room temperature [15,16,30]. The structural, thermal, and magnetic properties of these three ferromagnetic materials are listed in Table 5.

1.5. Theoretic Irradiation Tolerance of MTJs

Radiation induced damages on electronic circuits have been known since the 1950s. In the 1970s, memory and logic perturbations were detected in satellite electronic devices as a result of heavy-ion radiation within the solar wind [130]. Subsequently, soft errors caused by cosmic rays were reported in Si-based DRAM memory chips at the end of the 1990s [131]. Serving as a counterpart to Si-based devices, the stability of MTJ devices has also been investigated. In this subsection, the theoretical work will be discussed, while the experimental research will be covered in the subsequent section.

Theoretical investigations of the irradiation effects on MTJs were initially carried out using the Julliére model [18] and the theory of electron tunneling, both of which established TMR models. In this subsection, the Julliére model will be first discussed, followed by the electron tunneling model

According to a report in 1997 [132], the Julliére model is more suitable for amorphous barriers, not a precise representation of the magnetoconductance exhibited by free electrons tunneling through a crystalline barrier. Instead, in the case of thick barriers, Slonczewski's model may offer a more accurate approximation. Ionizing radiation, such as γ -rays, can displace atoms and create local lattice disorder, leading to the formation of amorphous regions in barrier layers. Therefore, despite this limitation, the Julliére model is employed here to illustrate the effect of an amorphous state in barrier layers, which is induced by irradiation. The model would offer a simplified visual representation of the degradation caused by irradiation.

Table 5. Physical properties of free-/fixed layer materials in MgO-based MTJs.

Property	Fe	Co	(Co,Fe) ₈₀ B ₂₀
space group	Im $\bar{3}$ m	P6 ₃ /mmc	amorphous [126]
density (g/cm ³)	7.87	8.90	7.29
melting point (K)	1,811	1,768	663–808* [127]
boiling point (K)	3,134	3,200	n/a
thermal conductivity (W/m/K)	80.4	100	n/a
electron configuration	[Ar]3d ⁶ 4s ²	[Ar]3d ⁷ 4s ²	n/a
electric conductivity (S / m at RT)	1.60×10^7	1.04×10^7	$10^6 - 10^8$ [128]
magnetic moment (μ_B)	2.2	1.6	2.1–2.5 [129]
Curie temperature (K)	1,043	1,388	631

from <https://www.periodic-table.org> and metglas.com.

*: crystallization temperature.

In non-magnetic materials, the populations of spin-up electrons and spin-down electrons are equal, which are randomly distributed in an equilibrium state. Conversely, in ferromagnetic materials, electron spins are aligned spontaneously, resulting in unequal numbers of spin-up and spin-down electrons. The unequal spin-up and spin-down electrons can tunnel into the empty states of the initial spin channel, which affect electrical resistance under magnetic fields, resulting non-zero MR ratios. The MR ratios of an MTJ can be expressed in terms of the conduction electron spin-polarization P_i of the ferromagnetic layers. [18,133]

$$\text{TMR Ratio} = \frac{2P_1 P_2}{1 - P_1 P_2} \quad (2)$$

where

$$P_i = \frac{D_{i,\uparrow}(E_F) - D_{i,\downarrow}(E_F)}{D_{i,\uparrow}(E_F) + D_{i,\downarrow}(E_F)} \quad (3)$$

Here $i = 1, 2$. $D_{i,\uparrow}(E_F)$ and $D_{i,\downarrow}(E_F)$ are the spin-dependent densities of states of the free-/fixed layers at the Fermi energy (E_F) for the majority-spin and minority spin bands. The spin-polarization of the free-/fixed layers P_i ($i = 1, 2$) is affected by free-/fixed layer materials. Based on the Jullière model, any factors changing the Bloch states (such as momentum and coherency) within the free-/fixed layer can affect tunneling probabilities and change the TMR ratios.

The concept of electron tunneling can explain MTJ too, with a particular focus on crystalline barrier MgO-based MTJs [134,135]. It is generally accepted that the effectiveness of MgO-based MTJs is highly dependent on the crystallinity of the insulting MgO barrier.

Figure 7 illustrates schematically coherent tunneling transports in MgO(001)-based MTJs. As illustrated in the schematics, there are three kinds of evanescent states (also known as tunneling states) for ideal coherent tunneling in the band-gap of MgO(001): Δ_1 , Δ_2 , and Δ_5 . Δ_1 Bloch states are highly spin-polarized in the ferromagnetic layers, and tunneling probability is a function of κ_{\parallel} wave vectors. Theoretical studies suggested that the ferromagnetic Δ_1 states dominate the tunneling process through the MgO(001) barrier [134,135]. When the symmetries of tunneling wave functions are conserved, ferromagnetic Δ_1 Bloch states can couple with MgO Δ_1 evanescent states, which have the slowest decay and highest tunneling probability [134] along the [001] direction. The dominant tunneling channel for the parallel magnetic state is free-layer $\Delta_1 \leftrightarrow$ MgO $\Delta_1 \leftrightarrow$ fixed-layer Δ_1 . In the parallel magnetic states, the majority spin-conductance occurs dominantly at $\kappa_{\parallel} = 0$ because of the coherent tunneling of majority spin Δ_1 states. In contrast, for the minority spin-conductance in the parallel magnetic state and the conductance in the anti-parallel magnetic state, spikes of tunneling probability would appear at the finite κ_{\parallel} points. Although a finite tunneling current flows in the anti-parallel magnetic state, the tunneling conductance of the

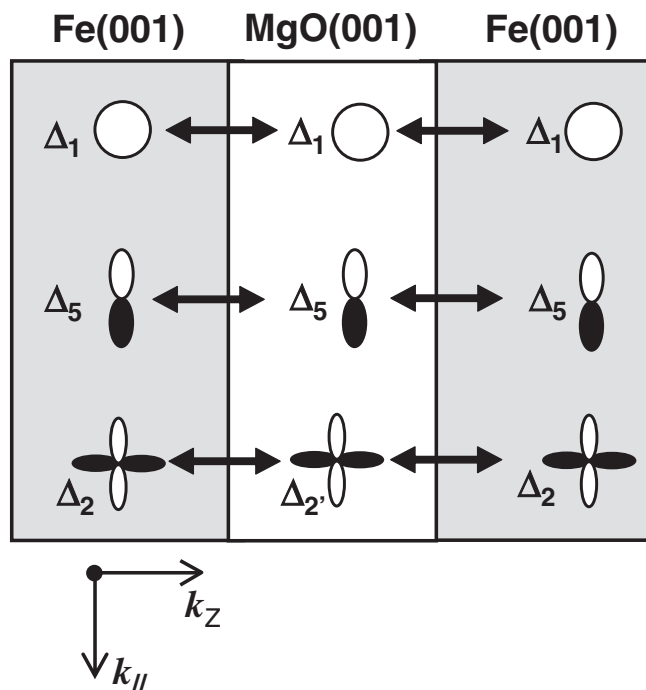


Figure 7. Coupling of wave functions between the Bloch states in ferromagnetic Fe(001) layers and the evanescent states in the MgO(001) barrier for $k_{\parallel} = 0$ direction. Δ_1 : $s - p - d$; Δ_2 : d ; Δ_5 : $p - d$. Reproduced with permission [15]. Copyright 2008, the Physical Society of Japan.

parallel magnetic state is much higher than that in the anti-parallel magnetic state, leading to a very high MR ratio.

According to the theory of electron tunneling, any modification to the symmetry of MgO barriers and ferromagnetic free-/fixed layers would affect the MR ratio of MgO-based MTJs. This means that the symmetry of both the propagating states in the magnetic layers and the evanescent state in the MgO barrier is critical in determining tunneling conductance. The symmetry matching of the Bloch actively controls the tunneling conductance and MR states in both the free-/fixed layers and the evanescent states in the barrier. Any changes to the symmetry of the MgO barrier and magnetic layers would affect the effective Δ_1 states between the MgO barrier and ferromagnetic layers, thereby changing the MR ratios.

As discussed above, several essential factors, including the crystallinity and crystallographic orientation of both the barrier and ferromagnetic layers, play essential roles in MR ratios. The presence of disorders, such as surface roughness, interface inter-diffusion, and impurities, as well as defects like grain boundaries, stacking faults, and vacancies, would significantly affect the spin-polarization and tunneling conductance.

Irradiation is a source to create defects in MTJs and potentially affect MR effects. Various types of ionizing radiations, such as α -particles, β -particles, and high-energy ions, as well as non-ionizing radiations including neutrons, electromagnetic radiation like γ -ray and X-ray, and thermal radiation, could degrade MR performances if any microstructures of MTJs are modified.

The radiation tolerance of AMR and GMR sensors has been experimentally investigated [136–138]. It was found that these sensors are generally somewhat radiation to resistant. The radiation tolerance of MTJ devices have also been experimentally studied. It was believed that polarization of the conduction currents and MR ratios of MTJs would be reduced if the interfaces between the tunneling oxide barrier and the ferromagnetic layer layers were damaged by radiation, which results in spin scattering defects [139]. Any permanent damage to the oxide barrier, usually caused by high-energy irradiation, would

cause leakage paths and reduce the tunneling resistance of MTJs. Low-energy irradiation would cause cumulative degradation of MTJs.

A recent review analyzed the effects of radiation on Al₂O₃-based MTJs [140]. High-energy heavy-ion irradiation usually caused the most displacement damage in this kind of MTJs, leading to deteriorated magnetotransport properties with increasing irradiation dose. High-energy protons and γ -ray irradiation have minimal effects on the magnetic properties of AlO-based MTJs, suggesting that AlO-based MTJs maybe a promising candidate for radiation applications.

Compared with oxide barriers in AlO-based MTJs, MgO barriers in MgO-based MTJs are thinner, which are usually 1 – 2 nm thick. The thinner crystalline layers would be more sensitive to irradiation, as observed in other two-dimensional materials [113,141], affecting performances of MgO-based MTJs significantly.

Here, we review the literature on the effects of irradiation on MgO-based MTJs, summarize published experimental data, and evaluate the resulting irradiation effects. This review will highlight the state-of-art findings of the effects of electromagnetic irradiation on MTJs with MgO barriers.

2. Effects of Cosmic Radiation

Primary cosmic rays and secondary high-energy cosmic rays include high-energy protons, alpha particles, nuclei, electrons, and various electromagnetic waves. Cosmic rays can be classified into four catalogs: heavy ions, mid-mass subatomic particles (proton and neutron), light-mass subatomic particles (electron), and massless electromagnetic waves. The effects of the first three kinds of cosmic irradiation are briefly reviewed in this section. The effects of electromagnetic irradiation will be reviewed in the subsequent section.

At sea level, the average annual cosmic ray dose is about 0.27 mSv (27 mrem). The irradiation dose is about 0.10 μ Sv/h. Cosmic radiation dose increases rapidly with increasing altitude, reaching about 2.0 μ Sv/h at 9 km altitude and about 9 μ Sv/h at 18 km altitude above the Earth's surface. Therefore, it is necessary to examine the cosmic irradiation on TMR-based MTJs utilized in daily life, especially in spacecrafts and satellites. It is generally accepted that the high-energy particle radiation, such as high-energy ions, neutron, proton, and electron, can degrade the performance of MgO-based MTJ devices.

2.1. High-energy Heavy-Ion Irradiation

Insulating oxide barriers can be degraded by heavy-ion radiations. It was reported that ultra-thin aluminum oxide tunnel barriers were damaged by highly charged ions (such as Xe ions with 19 – 42 keV) [142,142]. The conductance of AlO-based MTJs linearly increased with irradiation flux [114]. Furthermore, high-energy light ions (such as carbon and oxygen ions) and heavy ions (such as nickel ions) within 10 MeV decreased MR ratios of AlO-based MTJs irreversibly as the ion flux increased [143].

MTJ's MgO dielectric barriers are susceptible to radiation too. Typically, ionizing radiations usually generate charge trap centers in MgO barriers and the interfaces between MgO barriers and ferromagnetic layers. The produced charge-trap centers can lead to extra noise of MTJs [144] and reduce MR ratios of MTJs [145] by perturbing tunneling processes.

MTJ ferromagnetic materials are also susceptible to irradiation. It has been well known for decades that ion irradiation can damage crystallographic structures of MTJ ferromagnetic layer materials and change their physical properties [146]. Generally, ion irradiation would cause displacement damage, which affects the microstructure and properties linked to displacement damage [140]. It was reported that high-energy argon ions with 44 MeV and krypton ions with 35 MeV created amorphous zones [147] or defects [148] in BaFe₁₂O₁₉ magnetic materials, changing their magnetic properties and microstructures. High-energy helium-ion irradiation can create He nanobubbles at ion-implantation regions [149] and induce up to 36 % change in crystal anisotropy [150] of ferroelectric LiNbO₃ materials.

The radiation-induced damages of oxide barrier materials and ferromagnetic layer materials would affect behaviors of MTJ devices. It was reported that CoFeB / MgO

Table 6. Cosmic Radiation Irradiation of MgO-based MTJs.

MTJ structures	Irradiation conditions	Results	Ref.
CoFeB/MgO/CoFeB [†]	Fe ions, 15 MeV, 400 MeV; Ar, 250 MeV; Kr, 322 MeV; Xe, 454 MeV; Os, 490 MeV	soft errors were detected	[151]
CoFeB/MgO/CoFeB [§]	⁶⁰ Co, γ -ray, 247 - 475 Mrad, 220 rad/s, room temperature	magnetism was destroyed	[121]
CoFeB/MgO/CoFeB [#]	neutron, 0.1 eV - 10 MeV, 5×10^{10} particles / cm ² /s, 2.9×10^{15} particles cm ²	insensitive	[152]

Numbers in parentheses are nominal thicknesses in nm.

[†] Ta(5) / Ru(10) / Ta(5) / Pt(5) / [Co(0.4)Pt(0.4)]₆ / Co(0.4) / Ru(0.4) / [Co(0.4) / Pt(0.4)]₂ / Co(0.4) / Ta(0.3) / CoFeB(1) / MgO / CoFeB(1.5) / Ta(5) / Ru(5)

[§] Ru(8) / Ta(3) / Mg(0.75) / CoFeB(0.5) / W(0.2) / CoFeB(1.3) / MgO(0.8) / CoFeB(1.0) / W(0.25) / [Co/Pt]₃ / Co(0.6) / Ru(0.8) / Co(0.6) / [Co/Pt]₆ / [CuN/Ta] / Si

[#] Si / Ru(6) / IrMn(11) / CoFeB(6) / MgO(1.4) / CoFeB(5)

/ CoFeB MTJs were degraded by high-energy oxygen ion (O^-) irradiation during RF sputtering [153]. Table 6 lists some ion-irradiation effects on MgO-based MTJs. It is generally accepted that high-energy irradiation usually degrades TMR behaviors of MgO-based MTJs.

It was also reported that MgO-based MTJ devices exhibit irradiation tolerance. NASA conducted a tested MTJ-based MRAM (MR2A16A from Freescale Semiconductor Inc.) under heavy ion single event [112]. The tested MRAM exposed under 3.0 GeV Kr ions, 1.6 GeV Ar ions, and 3.2 GeV Xe ions. Test results indicated that the MRAM device was sensitive to Single Event Latchup (SEL), which was attributed to the complementary metal-oxide-semiconductor (CMOS) portion of the device. However, there was no indication that MTJ elements were damaged from heavy ions.

Radiation tolerance of MTJ devices was also reported by other research groups. Kobayashi *et al.* exposed CoFeB / MgO / CoFeB MTJs to high-energy Si-ion irradiation with 15 MeV [115]. The MTJs (consisted of Mg(1.3 nm) and CoFeB (1.5 nm) were sandwiched between 200 μ additional electrodes. Only minimal degradation ($\sim 1\%$) was observed in electrical resistance. However, no significant changes were detected in retention states before and after the irradiation.

2.2. High-energy Proton Irradiation

Hughes *et al.* irradiated MgO-based MTJ devices (MRAM) utilizing proton ions with energies up to 220 MeV and doses up to 1×10^{12} proton/m² [120]. The MTJ devices were consisted of Ru(7nm) / Cu(20nm) / Ta(5nm) / CoFeB(2.2nm) / MgO(1.2nm) / CoFeB(2.5nm) / Ru(1nm) / CoFe(2.5nm) / PtMn(15nm) / Ta(0.5nm) / Cu(100nm) / Ta(0.5nm) / SiO₂(100nm) / Si (substrate). Magnetization, ferromagnetic resonance, and tunnel magnetoresistance were examined before and after proton exposures. No changes were observed in their material properties. No radiation effects were observed.

Snoeck *et al.* exposed Au(~ 10 nm) / Pd(~ 20 nm / Fe(30nm) / MgO(0.6nm) / Fe(10nm) magnetic tunnel junctions under 150 keV nitrogen ions (N^+) at a flux of 5×10^{15} ions/cm² and 3×10^{16} ions/cm² [154]. Bi-linear and bi-quadratic coupling increased gradually with increasing ion dose. However, no completed description of the irradiation-induced effects was reported.

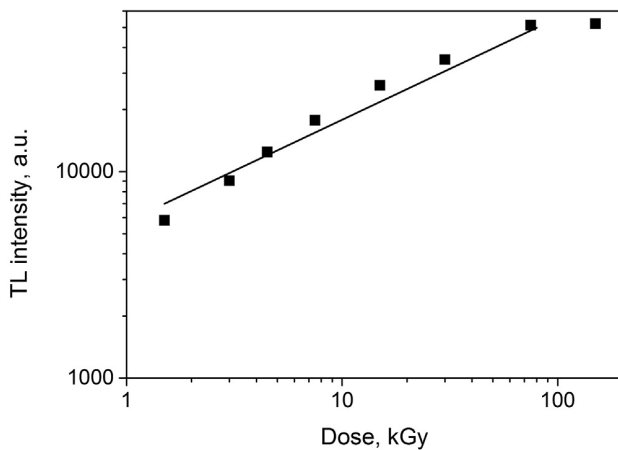


Figure 8. Dose dependence of TL intensity of MgO nanomaterials irradiated by a pulsed electron beam. Reproduced with permission [158]. Copyright 2015, Elsevier Ltd.

2.3. High-energy Neutron Irradiation

High-energy neutron irradiation usually alters atomic arrangements and damages crystalline structures of many materials. The irradiation can also create nanoscale amorphous regions within crystal lattices [155]. While metals are relatively immune to ionizing radiation due to their ionic bonds, fast neutrons can still enter metals and cause significant structural damages. For instance, neutron-irradiation induced defect clusters and cavities in copper [156], decreased magnetic remanences of NdFeB permanent magnets [116], and changed the Curie temperature of FeNiCrMoSiB amorphous alloys [157].

High-energy neutron irradiation can also damage the ferromagnetic layers of MgO-based MTJs. High-energy neutron can travel in the crystalline lattice of free-/fixed layers and displace these atoms from their initial lattice positions through kinetic energy transfer. This kind of displaced atoms are termed a primary knock-on atom (PKA). The PKA can continuously displace other lattice atoms that named secondary knock-on atoms (SKAs). This series of displacements can generate numerous defects in the crystalline free-/fixed layers, ultimately affecting the performance of TMJs. Table 6 lists one case of neutron irradiation, which is generally understood to degrade MTJ devices.

2.4. High-energy Electron Irradiation

High-energy electron irradiation affects MTJ component materials. In one study, amorphous CoFeB thin films (which are used as free-/fixed layers of TMJs) were exposed to electron-beam with an energy of 200 keV in a transmission electron microscope [117]. The electron radiation modified phase and microstructure of the films. Another study examined thermoluminescent properties of ultrafine MgO particles with size of 250 – 500 nm under high-dose electron irradiation [158]. A pulsed electron beam with 130 keV was employed at room temperature, with a pulse duration of 2 ns and current density of 60 A/cm². The absorbed dose was 1.5 kGy/pulse. Figure 8 shows the dose-dependent thermoluminescent (TL) intensity of the electron-irradiated MgO nanomaterials. Clearly, MgO structure should be modified by the electron irradiation.

Unfortunately, there have been few studies on the irradiation effects of high-energy electron on MgO-based MTJs. Metal layers are usually deposited over ferromagnetic layers of MTJs, preventing electrons from penetrating into MgO barriers and magnetic layers of MTJs. Therefore, high-energy electron should not affect MTJs due to the screen effects of metal layers.

3. Effects of γ -ray Irradiation

γ -rays are one kind of electromagnetic radiation with wavelengths ranging from 3×10^{-13} m to 3×10^{-11} m (approximately 40 keV to 4.0 MeV), being an ionizing radiation.

Table 7. γ -ray Electromagnetic Irradiation of MgO-based MTJs.

MTJ structures	Irradiation conditions	Results	Ref.
MgO crystals	3.0×10^6 rad/h for 20 min, ^{60}Co , 38 °C, measured within 2 min after irradiation	irradiation produced vacancies	[159]
MgO crystals	γ -ray, 2.1 MeV, up to 10 Mrad, 1.6×10^6 rad/h, RT	thermal conductivity decreased half; absorption increased five times; fully recovered after annealing at 625 °C for 1 h	[160]
MgO crystals ^T	γ -ray, 1.25 MeV, 10×10^4 Gy, 0.8 Gy/s, 450 K	TSL intensity increased linearly with dose	[161]
MgO crystals [⊥]	γ -ray, 1.25 MeV, 10×10^4 Gy, 0.8 Gy/s, 450 K	TSL intensity was very weakly dependent on dose	[161]
MgO powder	γ -ray (^{60}Co), 0.3 Mrads/h, ~ 20 Mrads, stored at RT for 1 year before measurement	TL changed after irradiation	[162]
MgO powder	γ -ray (^{60}Co), 8.33 mGy/s, 1 Gy - 50 kGy	TL changed with dose	[163]
Ag/MgO/Ag [▽]	γ -ray, 0.662 MeV, up to 32.55 mGy	capacitance increased with dose	[122]
CoFeB films	γ -ray, 1.2 MeV, 2.58×10^5 C/kg, 60 °C	sensitive to γ irradiation	[119]
MgO/CoFeB [§]	γ -ray, 100 kRad	no noticeable change in magnetic properties	[164]
CoFeB/MgO/CoFeB	^{60}Co , γ -ray, 1 Mrad	no effect	[120]
CoFeB/MgO/CoFeB [¶]	^{60}Co , γ -ray, 10 Mrad, 9.78 rad/min	highly tolerant of γ -radiation	[152]
CoFeB/MgO/CoFeB [‡]	^{60}Co , γ -ray, below 20 Mrad, 220 rad/s, RT	coercivity increased with irradiation while saturation magnetization was not affected	[121]

Numbers in parentheses are nominal thicknesses in nm.

^T MgO crystals with OH⁻ impurity of $(4.7 - 4.9) \times 10^{17} / \text{cm}^3$.

[⊥] MgO crystals without OH⁻ impurity.

[▽] Ag / MgO thick film / Ag. Grain size of MgO particles: 0.5 – 1.0 μm . Ag was electrode.

[§] Ru(7) / Ta(10) / Co₆₀Fe₂₀B₂₀(3) / Mg(0.3) / MgO(1.1) / Co₆₀Fe₂₀B₂₀(3) / Ru(0.8) / Co₇₀Fe₃₀(2.5) / PtMn(20) / Ta(5) / CuN(30) / Ta(5)

[¶] CoFeB(5) / MgO(1.4) / CoFeB(6) / IrMn(11) / Ru(6)

[‡] [Co(0.5) / Pt(0.2)]₆ / Co(0.6) / Ru(0.8) / Co(0.6) / [Co(0.5) / Pt(0.2)]₃ / W(0.25) / CoFeB(1.0) / MgO(0.8) / CoFeB(1.3) / W(0.2) / CoFeB(0.5) / MgO(0.75) / Ta(3.0) / Ru(8.0)

RT: room temperature; TSL: thermally-stimulated luminescence.

The electromagnetic wave can penetrate materials deeply and interact with matters through three kinds of primary processes: photoelectric effect, Compton scattering, and electron-positron pair production, depending on the energy of the incident γ -ray. When the energy of γ -ray is higher than 1.02 MeV, it may spontaneously produce an electron and positron pair. Compton scattering is the principal mechanism when the energy of γ -ray is 40 keV – 4.0 MeV. The photoelectric effect dominants when the energy of γ -ray is below 50 keV, whereby an electron absorbs the incident γ -ray and is excited to conduction bands. In all three kinds of processes, γ -ray collides inelastically with electrons, losing energy and continuously moving with a longer wavelength. Furthermore, γ -ray can directly ionize atoms through the photoelectric effect and the Compton effect and indirectly through secondary ionization. These processes occur when MTJs are exposed to γ -ray.

Depending on γ -ray's energy and properties of MTJ materials, γ -ray can induce displacements of atoms within lattice, termed defects. These defects can remain for a long time at room temperature and can be investigated from the Hall effect and electrical measurements. This kind of irradiation-reduced defects would affect the performances of MTJs. In facts, most degraded MTJs were investigated under this kind of irradiation interaction.

In contrast to the above interactions, γ may only disturb atoms of MTJ materials intermittently or transiently. The produced disturbances of atoms may disappear shortly once γ -ray is removed. This kind irradiation-induced degradation can be only *in-situ* real-time detectable while under irradiation.

Experimental investigations supported these two kinds of γ -ray interactions. Several groups have reported that MgO-based MTJs are highly tolerant of γ -ray radiation up to a dose of 10 Mrad [152,165]. In their work, MTJs were irradiated and then measured *ex-situ*. Their results indicated that γ -ray irradiation did not noticeably change TMR ratio, coercivity, and magnetostatic coupling of low-frequency noise. As such, MgO-based MTJ devices are expected to operate reliably in γ -ray radiation environment, especially at doses below a few hundred Rad [166]. Other scientists hold a view that γ -ray irradiation should degrade MgO-based MTJ devices because γ -ray changed microstructures of MTJ materials [161]. Additionally, others suggested that γ -ray radiation may affect peripheral circuits of MgO-based MTJ devices (not MTJs) during the read/write operation, leading to soft-errors [167].

Table 7 lists some results of γ -ray irradiation. In the following subsections, these published data will be analyzed in details with respect to the MTJ structures and experimental conditions, including the conditions of γ -ray irradiation and measurement methods. First, the physical properties of γ -irradiated MTJ material, including MgO crystals (used as barriers in MTJs), fixed-layers and free-layers, and MgO / ferromagnetic layer interfaces, will be reviewed first. Next, the review will focus on physical properties of γ -irradiated MgO-based MTJs. Finally, the tolerance ability of MgO-based MTJs will be discussed from γ -ray penetration in MTJs and MTJ devices to explore potential explanations of MgO-based MTJs' irradiation tolerance.

3.1. MTJ Materials under γ -irradiation

MgO-based MTJs consist of MgO barriers, ferromagnetic free- / fixed-layers, and metal electrodes. The performance of MTJs is influenced by microstructures, physical properties, and interfaces of these MTJ materials. Therefore, the characteristics of these MTJ materials with respect to γ -ray irradiation are discussed firstly.

3.1.1. MgO Crystals under γ -irradiation

There is limited amount of literature available on the effects of γ -ray damage on MgO barriers with nanometer thickness [140]. To ensure adequate information on γ -ray irradiated MgO materials, the irradiation properties of MgO bulks and thick-films are

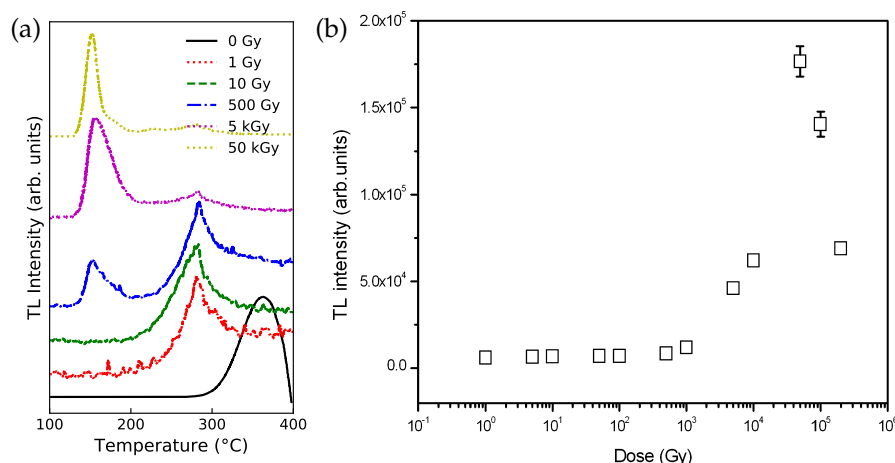


Figure 9. (a) TL intensity of MgO powders irradiated by gamma-ray. Replotted from [163]. (b) TL response of MgO powders with gamma dose. Reproduced with permission [163]. Copyright 2009, Taylor & Francis Group.

reviewed here. It is expected that the irradiation properties of MgO barriers in nanometers will exhibit similar behaviors to these observed in MgO bulks and thick-films.

Irradiation properties of MgO have been investigated since the 1960s to explore the potential of MgO for γ -ray dosimetry by studying its response to γ -ray irradiation. MgO crystals were cleaved from ingots and exposed to ^{60}Co sources with a radiation intensity of $3.0 \times 10^6 \text{ R/h}$ [159]. Thermoluminescence indicated that γ -ray irradiation induced defects in MgO crystals.

MgO powders were also irradiated by γ -ray lately. Kiesh *et al.* exposed commercial MgO powders to ^{60}Co γ -ray irradiation with a total dose of 20 Mrads [162]. The irradiated powders were then kept at room temperature for over a year before measurements. The results showed that γ -irradiation caused a shift of thermoluminescence peaks. In another study, MgO powders with a purity of 99.9 % were exposed to γ -irradiation using a ^{60}Co source with a dose rate of 8.33 mGy/s [163]. Figure 9a shows thermoluminescence (TL) of the γ -ray irradiated MgO powders. Low-dose γ -irradiation induced a peak around 280 °C, while a high γ -irradiation dose (above 300 Gy) resulting in a peak at 150 °C which became dominant after exposure to dose above 1 kGy. It was believed that the irradiation dose affected the recombination centers and caused the shift of TL peaks. Figure 9b shows the relationship between γ -dose and TL response integrated across the entire TL curve over the dose range. The TL response changed linearly with irradiation dose at intermediate dose levels of 1 – 100 Gy, while sub-linearly at higher dose levels of 0.5 – 50 kGy.

Arshak *et al.* investigated MgO capacitors consisted of Ag electrodes and sandwiched MgO thick films [122,168]. The grain size of the MgO particles was 0.5 – 1.0 μm . These MgO capacitors were exposed to γ -ray irradiation with a maximum dose of 32.55 mGy and an energy of 0.662 MeV. Figure 10 shows a real-time capacitance of the MgO capacitors as a function of γ -ray radiation dose. The capacitance increased continuously with γ -ray dose, being reversible and less susceptible to γ -ray radiation. γ -rays should damaged the MgO particles and produced structural defects (such as color centers or oxygen vacancies) in MgO, changing the density of charge carriers of the MgO films.

Steinike *et al.* exposed mechanically cleavage MgO samples to γ -ray emitted from ^{60}Co sources [169]. The irradiation was carried out at a rate of 3.4 – 4.5 MRad/h and energy 1.25 MeV at –196 °C. γ -ray irradiation generated F^+ -centers and V^- centers in the MgO crystals. The concentrations of F^+ and V^- centers increased linearly with irradiation doses up to 1 – 3 MRad, followed by saturation at higher doses. Additionally, the concentration of the F^+ defect centers decreased with increasing annealing temperature and the F^+ enters could be removed by annealing at 600 °C.

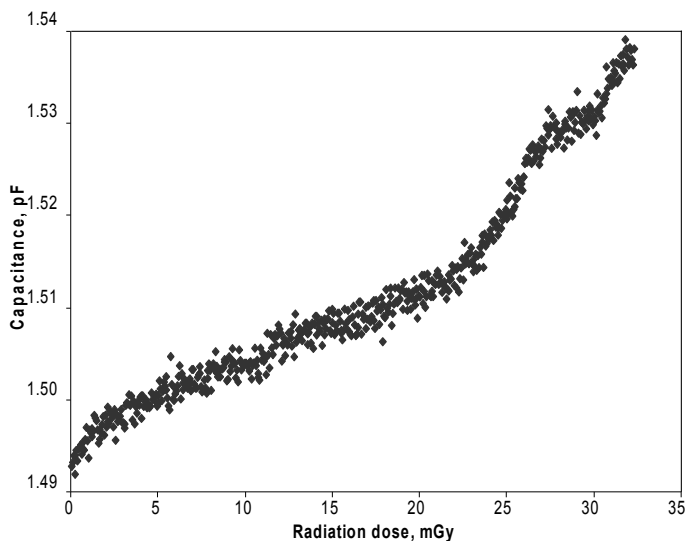


Figure 10. Real-time capacitance versus γ -ray radiation dose for Ag / MgO / Ag capacitors. Reproduced with permission [122]. Copyright 2005, Springer.

Clement *et al.* *in-situ* studied absorption and luminescence spectra of MgO crystals under γ -ray irradiation [170]. MgO crystals with 99.99 % purity were exposed to γ -ray at a flux of 3.5×10^4 rad/h for 7 h at 20 °C and 120 °C, in a vacuum of less than 2×10^{-6} Torr. The real-time absorption increased with increasing irradiation dose at both temperatures. It was also reported that subsequent annealing at 600 °C cancelled the irradiation effect. Based on the results, it was concluded that impurities of Fe (less than 300 ppm) and Cr (less than 100 ppm) played a significant role in the degradation caused by irradiation.

Abramishvili *et al.* studied γ -ray irradiated MgO crystals too [160]. The total impurity content in the crystals did not exceed 245 ppm. The irradiation was carried out at room temperature, with a dose of 1.6×10^6 rd/h and a maximum γ -ray energy of 2.1 MeV. *In-situ* measurements were performed at low temperatures. It was observed that the irradiation significantly changed the thermal conductivity of the MgO crystals, as shown in Figure 11a. The thermal conductivity was partially reversed by annealing the irradiated crystals at 515 °C for one hour, which led to the recovery of the crystals' heat conductivity to their initial state. The observed reversal is consistent with other reports [170]. Additionally, their optical absorption was changed after irradiation, as shown in Figure 11b. Upon further analysis, it was believed that γ -ray irradiation caused the formation of Frenkel pair defects, which changed both thermal conductivity and optical absorption. Frenkel pair defects can be eliminated through annealing, which leads to the restoration of the original thermal conductivity.

Kvatchadze *et al.* *ex-situ* measured thermo-stimulated luminescence (TSL) of nominally pure MgO single crystals containing few impurities (Cr^{3+} : 12 – 26 ppm; Mn^{2+} : 35 – 72 ppm; V^{2+} : 24 – 60 ppm; and OH^- : 0 – $4.9 \times 10^{17} \text{ cm}^{-3}$) under γ -ray irradiation (0.8 Gy/s and 1.25 MeV) over a temperature range of 300 K to 775 K [161]. It was reported that in MgO crystals containing OH^- impurities, the TSL intensity steadily increased with increasing γ -ray radiation dose at 450 K, as shown in Figure 12a. Additionally, the TSL intensity at 450 K increased linearly with the γ -ray radiation dose (Figure 12b). However, in MgO crystals without OH^- impurities, the TSL intensity at 450 K is extremely low sensitive to γ -ray irradiation (Figure 12b). It was believed that foreign hydroxyl ions trapped charges in γ -ray irradiated MgO crystals, inducing accumulation of hole centers to change optical properties.

Lynch *et al.* *in-situ* investigated photoconductivities of MgO polycrystalline bulks under γ -ray irradiation fields over a temperature range of 300 K to 600 K [171]. γ -rays were emitted from a ^{60}Co source, with energy of 1.17 MeV or 1.33 MeV. It was reported that the photo-conductivity of MgO bulks increased linearly with γ -ray radiation dose.

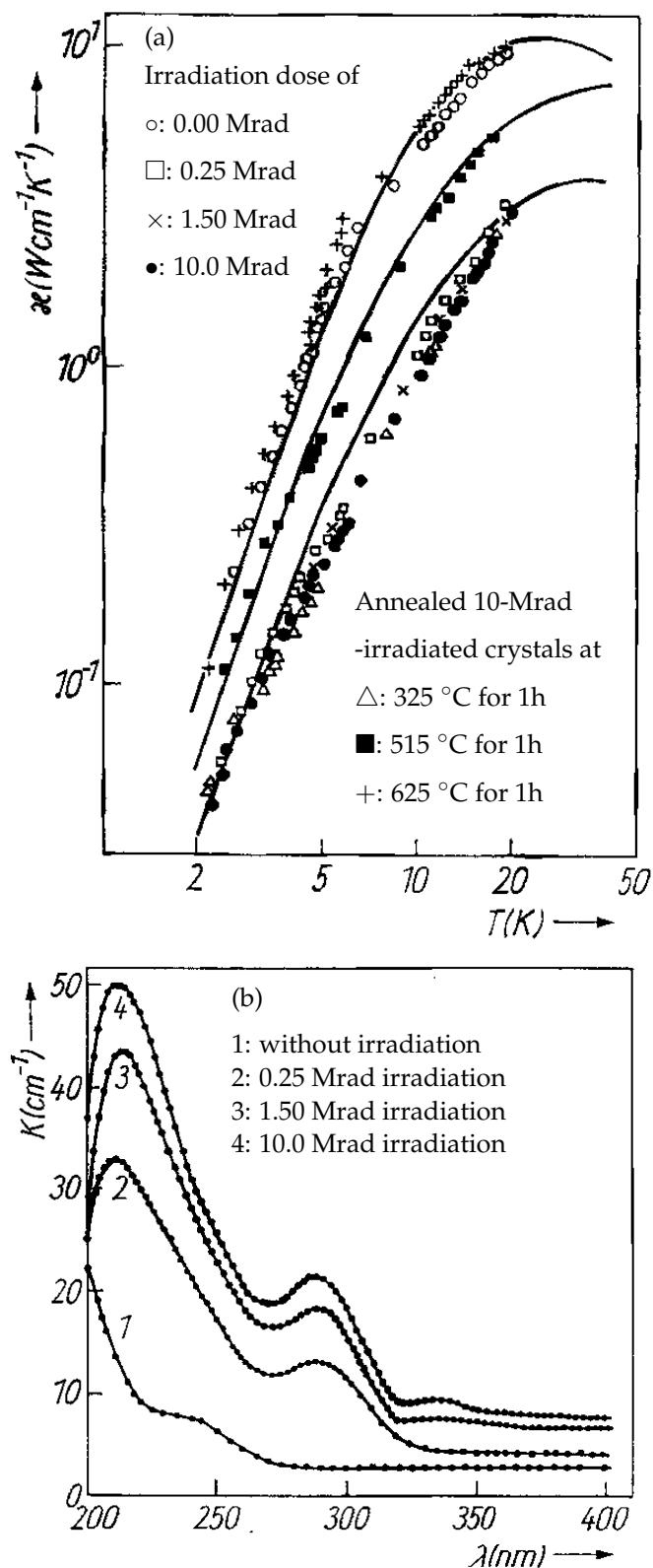


Figure 11. (a) Thermal conductivity and (b) Spectra of optical absorption of MgO crystals before and after γ -irradiation. Reproduced with permission [160]. Copyright 1981, John Wiley and Sons.

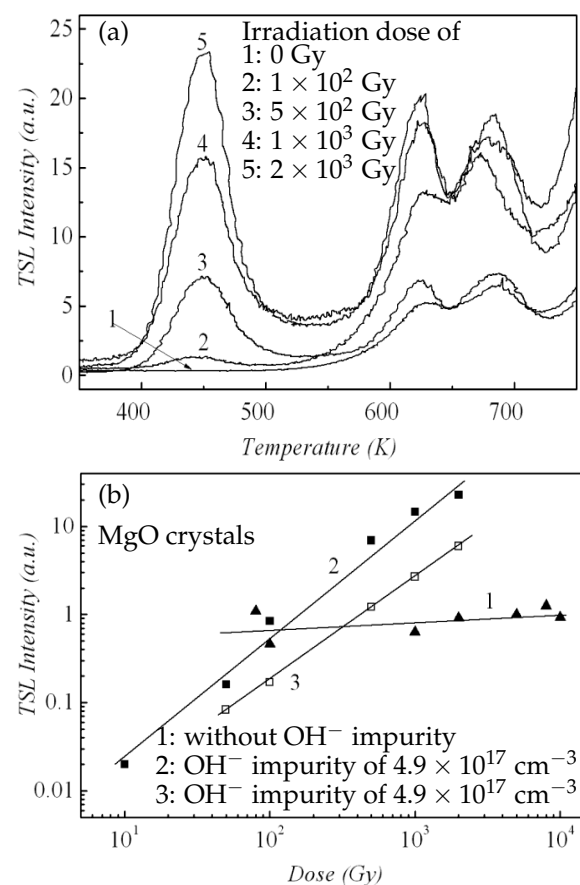


Figure 12. (a) TSL curves of MgO single crystals with OH^- impurity of $4.9 \times 10^{17} \text{ cm}^{-3}$ under γ -irradiation under different temperatures. (b) TSL intensity dependence of γ -irradiation dose at 450 K. Reproduced with permission [161]. Copyright 2011, David Publishing Company.

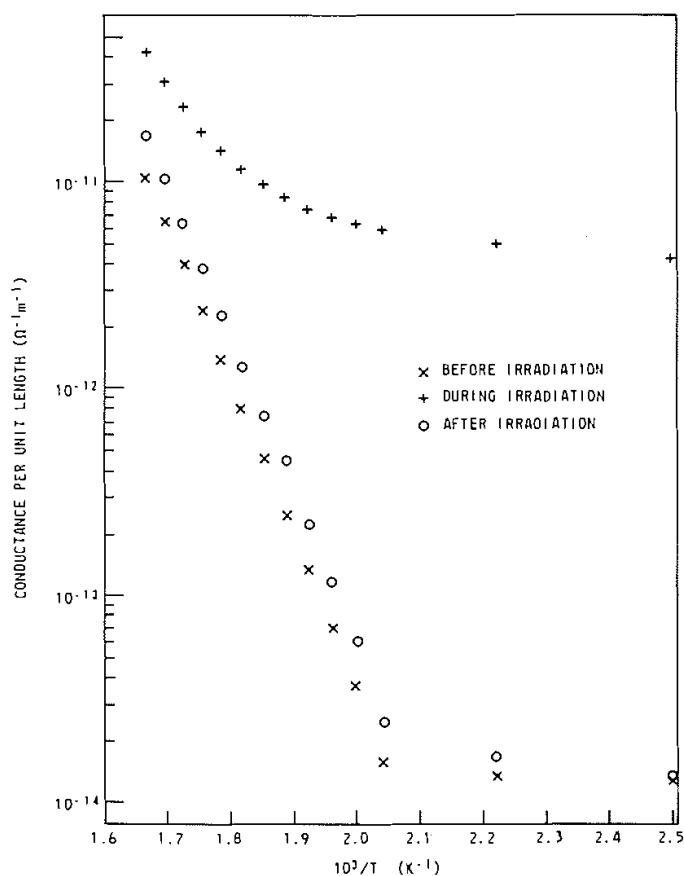


Figure 13. Temperature-dependent photoconductance per unit length of MgO polycrystals before, during, and after γ -ray irradiation. Reproduced with permission [171]. Copyright 1975, Canadian Science Publishing.

The γ -ray induced conductivity showed a linear dependence on the radiation dose rate up to 4.0×10^5 rad/h. Additionally, the photo-conductance of MgO bulks increased by about three orders of magnitude when exposed to a γ -ray irradiation with flux of $(2.9 - 3.7) \times 10^5$ rad/h.

The studies described above have demonstrated the sensitivity of MgO materials (single crystals, polycrystalline bulks, mechanically exfoliated layers, and powders) to γ -ray irradiation. *In-situ* work indicated that the irradiation-induced defects could be restored to initial states of non-irradiated states, especially after being annealed at high temperatures.

The thickness of MgO crystalline films employed as barrier layers in MgO-based MTJ devices are only several nanometers. Such kinds of thin layers are expected to be more sensitive to γ -ray irradiation than their bulk counterparts to γ -ray irradiation, as observed in other two-dimensional nanolayers [113]. As a result, MgO-based MTJs should be sensitive to γ -ray if MgO layers are exposed to γ -ray irradiation.

Different from free-standing MgO films, MgO barrier layers are sandwiched between ferromagnetic free-/fixed layers in MTJs. The ferromagnetic layers could potentially reduce irradiation dose into MgO barrier layers and provide some levels of protection. Furthermore, defects induced by γ -ray irradiation may be intermittent and disappear shortly after irradiation exposure or thermal annealing. Therefore, the irradiation effect on MgO barrier layers are more complex than discussed above. *In-situ* and real-time measurements should be required to examine the effect of γ -ray irradiation on MgO barrier layers.

3.1.2. Ferromagnetic Materials of MTJs under γ -irradiation

Ferromagnetic films are utilized in MTJs to sandwich MgO barrier layers, with one being the fixed-layer and the other being the free-layers. These ferromagnetic layers are typically made of Fe(001) films, FeCo films, or CoFeB films. A typical MTJ consists of Si / SiO₂ / Ta(5) / Ru(10) / Ta(5) / Co₂₀Fe₆₀B₂₀(5) / MgO(2.1) / Co₂₀Fe₆₀B₂₀(3) / Ta(5) / Ru(5) (where the numbers in parentheses denote the thickness in nanometers) [172]. Unlike MgO barrier layers with a thickness of 1-2 nanometers, the ferromagnetic layers, such as CoFeB, are thick and the performance of MTJs is closely related to their magnetic properties.

Wang *et al.* [121] investigated CoFeB / MgO perpendicular-anisotropy magnetic tunnel junction and found that the magnetism was destroyed if the irradiation dose was sufficiently high.

Shkapa *et al.* exposed FeCoB metallic ribbons to γ -ray irradiation and examined their magnetic properties using nuclear magnetic resonance and the Mössbauer effect [119]. The (Co, Fe)₈₅B₁₅ metal glasses were irradiated by 1.2 MeV γ -ray at 60 °C. It was reported that Co_{85-x}Fe_xB₁₅ ($x = 12 - 25$) magnetic glasses were sensitive to γ -irradiation, changing the atomic short-ordering of FeCoB ribbons.

Other ferromagnetic materials, such as Fe, Co, and FeCo alloys, should be similar to CoFeB materials under γ -ray irradiation. To ensure the similarity, the displacements per atom cross-section of Fe films with size of 100 nm × 3 μ m × 12 μ m was calculated using the Monte Carlo simulation method [173] under γ -ray with energy of 1.3 MeV and source activity of 1000 Ci. The displacement cross-section is 0.1 barns. The calculation indicated that the atomic displacement rate was about 0.6/s. Furthermore, γ -ray induced displacement cross-sections were very low for γ -ray irradiation with energy > 1 MeV.

Besides MgO barrier layers and ferromagnetic layers, non-magnetic metal films in MTJs, like Ta and Ru layers, can protect MgO layers and ferromagnetic films from γ -ray irradiation. However, the consequences of γ -ray irradiation on metal films are not the subject of this review. Although not discussed here, there is literature available on this topic [174].

3.1.3. Interfaces of MgO Barrier / Ferromagnetic Layers

The performance of MTJs is influenced by interfaces between MgO barriers and ferromagnetic layers. Recent investigations have showed that CoFeB can form Co(Fe)-O bonds and bond to MgO epitaxial grains after annealing [172]. Conversion electron Mössbauer spectroscopy studies indicated that interfaces between MgO(001) and Fe(001) layers were partially oxidized over 60 %, and Fe diffused into MgO barriers from both ferromagnetic interfaces [175]. It is suggested that these interfaces may be more sensitive to γ -ray irradiation, similar to Al₂O₃-based MTJs, whose physical properties were significantly affected by irradiation [140].

Recent *in-situ* experiments discovered that the uniaxial magnetic anisotropy decreased systematically with increasing annealing temperature [176]. Specifically, the MgO / FeCoB / MgO layers becomes isotropic after annealing at 450 °C. The asymmetry at the interfaces was explained by the diffusion of boron from the FeCoB interface layer into the adjacent MgO layer. Electronic structures of MgO/Fe interfaces have been investigated [177]. It is believed that Fe 3d -O 2p hybridization and distortion of the Fe film play important roles in magnetic anisotropy at the MgO/Fe interface.

Thermal annealing also affects interfaces between MgO barriers and ferromagnetic layers. The details are discussed in the section of Infrared Irradiation and Thermal Annealing.

3.2. MTJs under γ -irradiation

Until this point in time, there have been two distinct viewpoints regarding the impact of γ -ray radiation on MgO-based MTJs. Some scientists believe that MgO-based MTJs are susceptible to γ -ray radiation and are likely to sustain damage as a result. Other scientists argue that MgO-based MTJs are resilient to γ -ray radiation. In the following subsections, each of these viewpoints will be reviewed in detail.

3.2.1. Sensitive Results

Considering the reported irradiation properties of MgO barrier materials and the discussion on ferromagnetic layer materials of MgO-based MTJs above, it can be inferred that MgO-based MTJs would be affected by γ -ray irradiation. However, there are limited reports on the degradation of MgO-based MTJs under γ -ray irradiation. Two sensitive cases are reviewed below.

Wang *et al.* measured magnetic properties of double-interface CoFeB / MgO perpendicular anisotropy magnetic tunnel junctions (p-MTJ) [121]. The MTJ films were deposited on thermally oxidized Si substrates with CuN / Ta seed layers, consisting of [Co(0.5) / Pt(0.2)]₆ / Co(0.6) / Ru(0.8) / Co(0.6) / [Co(0.5) / Pt(0.2)]₃ / W(0.25) / CoFeB(1.0) / MgO(0.8) / CoFeB(1.3) / W(0.2) / CoFeB(0.5) / MgO(0.75) / Ta(3.0) / Ru(8.0) (numbers in parenthesis are thickness in nanometers). The CoFeB / MgO p-MTJs were exposed to a Cobalt-60 γ -ray irradiation at room temperature with a dose rate of 220 rad/s. The results showed that the coercivity of the γ -ray irradiated p-MTJs increased gradually with increasing dose of up to 20 Mrad, as shown in Figure 14. However, there was no observed variation in the saturation magnetization.

It was reported that the magnetism of MgO-based MTJs was destroyed by γ -ray irradiation when the dose was sufficiently high to 247 Mrad [121]. It was hypothesized that the destruction of magnetism was caused by radiation-induced thermal stress. Figure 15 shows the surfaces of the MTJs after γ -ray irradiation, which was caused by differences in thermal expansion coefficients between the MTJ films and the substrate.

3.2.2. Tolerant Results

Numerous research groups have reported high tolerance of MgO-based MTJs to γ -ray radiation, with no observed impacts on magnetic or electrical properties of MgO-based MTJs.

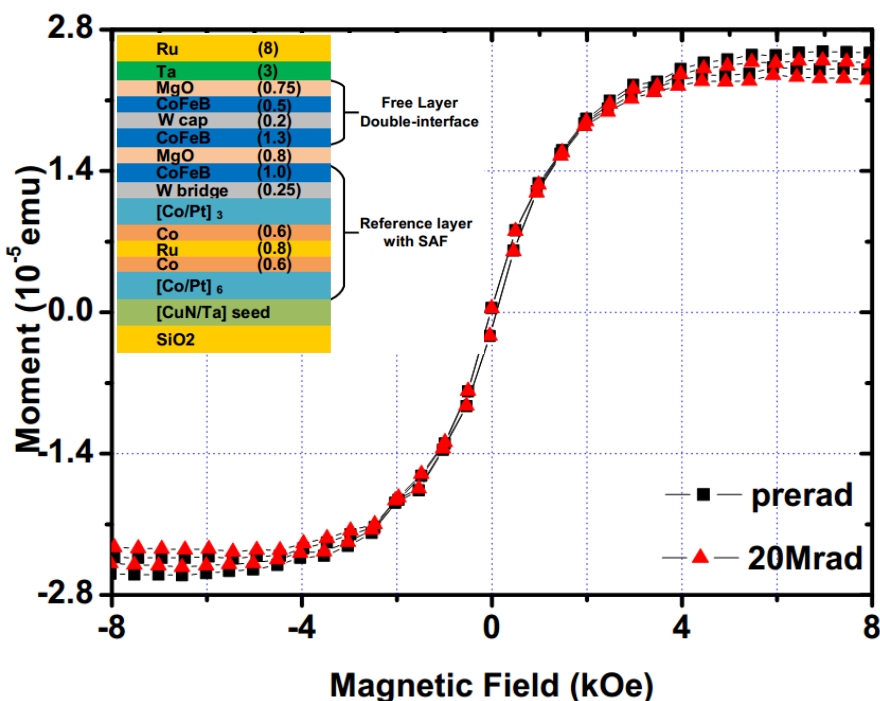


Figure 14. M-H hysteresis loops of MgO-based MTJs measured in an in-plane magnetic field before and after irradiation with a TID of 20 Mrad (Si). Reproduced with permission [121]. Copyright 2019, IEEE.

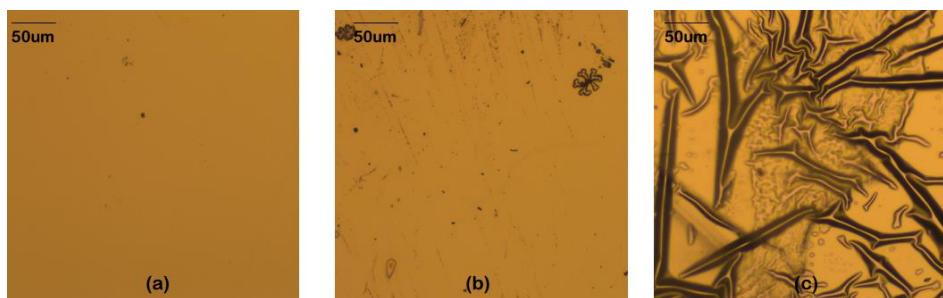


Figure 15. Optical surface images of MgO-based MTJs (a) before irradiation, (b) after 20 Mrad (Si) irradiation, and (c) after 247 Mrad (Si) irradiation. Reproduced with permission [121]. Copyright 2019, IEEE.

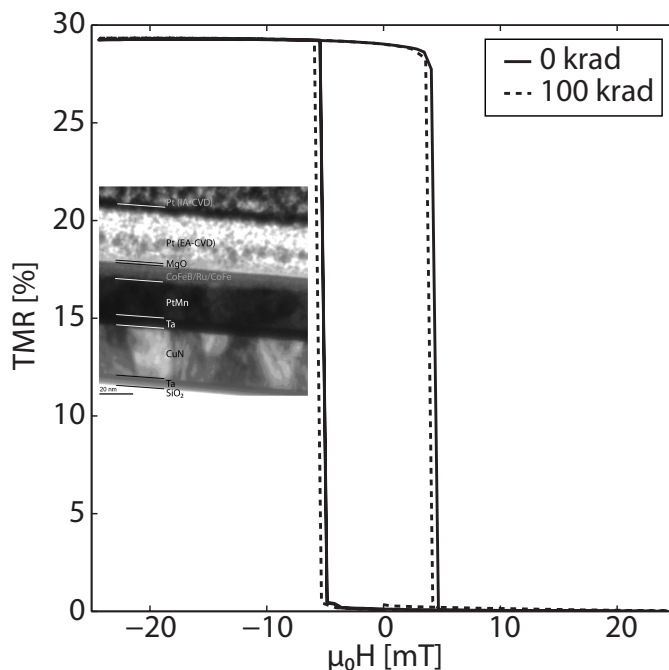


Figure 16. TMR of a single MgO-based MTJ before and after irradiation. Inset: Cross-sectional TEM image. Reproduced with permission [164]. Copyright 2010, International Training Institute for Materials Science. Reproduced with permission [165]. Copyright 2011, IOP Publishing Ltd.

Nguyen *et al.* exposed a bare MTJ to γ -ray irradiation (1.25 MeV) for a total ionizing dose of 100 kRad [164]. The MTJ consisted of Ru(7) / Ta(10) / Co₆₀Fe₂₀B₂₀(3) / Mg(0.3) / MgO(1.1) / Co₆₀Fe₂₀B₂₀(3) / Ru(0.8) / Co₇₀Fe₃₀(2.5) / PtMn (20) / Ta(5) / CuN(30) / Ta(5) (numbers in parenthesis are thickness in nanometers). *Ex-situ* measurements revealed that the dose of γ -ray irradiation did not cause any noticeable changes in magnetic properties of the MTJ, as shown in Figure 16. The MTJ exhibited no noticeable changes in either coercivity or magnetostatic coupling.

Ren *et al.* investigated MgO-based MTJs exposed to γ -ray irradiation [152]. The MTJs had a full structure of Si / Ru(6) / IrMn(11) / CoFeB(6) / MgO(1.4) / CoFeB(5) (numbers in parenthesis are thickness in nanometers), as shown in the inset of Figure 17a. The tunnel barrier was made of MgO with (001) crystalline orientation. The junction was exposed to ⁶⁰Co irradiation at a dose rate of 9.78 rad/min. Figure 17a shows the hysteresis loop of a single MTJ before and after exposure to the γ -radiation. A 10 MRad irradiation had a very weak effect on electrical resistances. Figure 17b shows coercive field H_c and TMR of other individual MTJs with the same structure that were tested under the same irradiation. The measured coercive field H_c and TMR were almost the same before and after γ -ray irradiation. Neither the electrical nor the magnetic properties of the MTJs were affected by the radiation. Therefore, the study concluded that MgO-based MTJs were highly tolerant of γ -radiation with a dose of 10 MRad at 1.25 MeV.

Hughes *et al.* exposed MgO-based MTJs to Co⁶⁰ γ -ray irradiation with a dose of up to 1 Mrad (Si) [120]. It was reported that γ -ray irradiation did not affect state retention and switching characteristics of MgO-based MTJs.

Most experimental measurements discussed above were carried out after γ -ray irradiation exposures, and it remained unclear whether the after-exposure status was equivalent to the exposure status. Nonetheless, it can be inferred that MgO-based MTJs are capable of retaining their non-irradiated initial status after γ -ray irradiation.

In addition to experimental studies, some theoretical research has been reported in support of the radiation tolerance of MgO-based MTJs. For instance, Kang *et al.* theoretically evaluated commercial CMOS non-volatile units and MgO-based *p*-MTJs [167]. Their

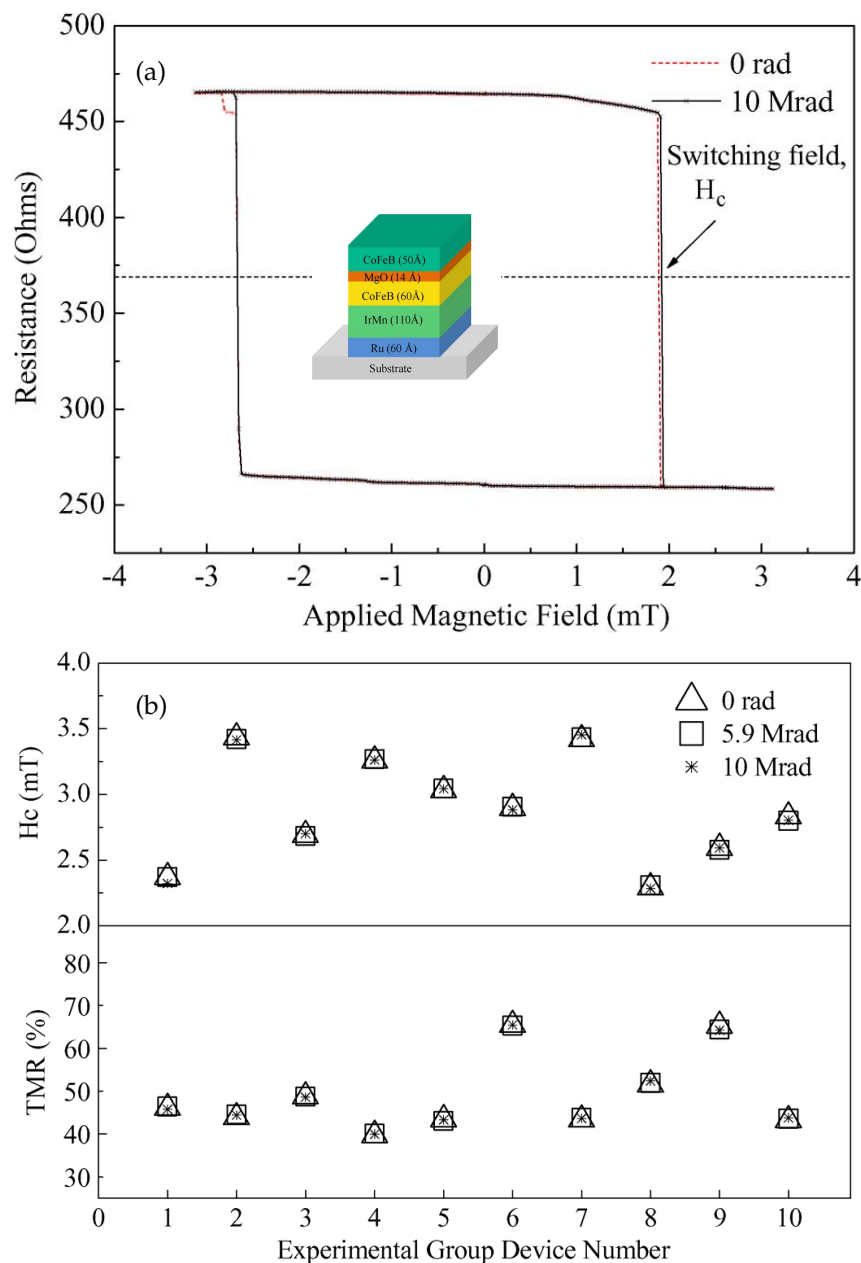


Figure 17. (a) Hysteresis loop of a single MgO-based MTJ and (b) H_c and TMR of a series of MgO-based MTJs before and after exposure to the γ -radiation with ~ 10 rad/s in dose rate and 1.25 MeV. Inset: Illustration of the MTJ stack. Reproduced with permission [152]. Copyright 2012, IEEE.

simulation results showed that CoFeB / MgO / CoFeB MTJs should be resistant to radiation effects.

3.3. Discussion on γ -irradiation of MTJs

As mentioned above, certain research groups have claimed that MgO-based MTJs are *in-situ* sensitive to γ -ray irradiation due to the sensitivity of MgO-barriers to γ -ray irradiation. On the other hand, most laboratories have reported that MgO-based MTJs are tolerant to γ -ray irradiation. In order to explain the discrepancy in the response of MgO-based MTJs to γ -ray irradiation, the effects of γ -ray are discussed below from γ -ray penetrations, dynamic behaviors of MTJ materials, and tunneling tolerance. The discrepancy may come from different experimental conditions.

3.3.1. γ -penetrations in MTJs

MTJs consist of MgO barrier layers sandwiched between ferromagnetic free- / fixed-layers, and metal electrodes, as well as electrodes made from high atomic number (high Z) materials with high-density like Ta and Au. Electromagnetic waves, including γ -rays, can pass through these metal and ferromagnetic layers to reach MgO barriers. In order to analyze these penetrations under different irradiation conditions, electromagnetic penetrations are calculated. The intensity of electromagnetic radiation inside MTJs decreases exponentially from MTJ's surfaces, as described by the equation based on the Beer-Lambert law [178,179]:

$$I = I_0 e^{-\mu z} \quad (4)$$

where I is the intensity of electromagnetic irradiation transmitted over a distance z , I_0 is the incident electromagnetic wave intensity, μ is the linear attenuation coefficient in cm^{-1} , $\mu = n\sigma = n(\sigma_{photoelectric} + \sigma_{Compton} + \sigma_{Pair})$ (n : the number of atoms/cm 3 ; σ : proportionality constant that reflects the probability of an electromagnetic wave photon being scattered or absorbed), and z is the distance traveled by the radiation in cm. For multi-layered films, the electromagnetic intensity is proportional to both the attenuation coefficient and the thickness of each layer through which it passes [180].

The calculation of electromagnetic radiation transmission through an MTJ is based on a typical MTJ structure consisting of Ta(5) / Ru(10) / Ta(5) / Co₂₀Fe₆₀B₂₀(5) / MgO(2) / Co₂₀Fe₆₀B₂₀(3) / Ta(5) / Ru(5) / Cr(10000) / Au(10000) (with numbers indicating nominal thicknesses in nanometers), as described in published literature [172,181]. The linear attenuation coefficients of each film material are obtained from published data and used in the calculation. Equation 4 is then applied to calculate the transmission of electromagnetic radiation through the MTJ device. Figure 18 shows the calculated electromagnetic irradiation intensity in the typical MTJ structure. The used electromagnetic radiation spans from 4.950 keV to 1 MeV in energy, covering both γ -ray (with energy greater than 124 keV) and X-ray (with energy of 125 eV - 125 keV) irradiation. According to the theoretical calculation, γ -ray could penetrate the entire MTJ structure without undergoing significant absorption.

Some MTJs may contain thick metal electrodes, which can affect the penetration of γ -rays through devices. Figure 19 shows the transmission of γ -rays through iron, a ferromagnetic material used in some MgO-based MTJs [2,175,182]. γ -rays can penetrate through iron for several centimeters, consistent with other reports [183]. Thus, γ -rays with various energy levels can easily penetrate entire MTJs, which consist of metal nano-films and thick electrodes, after passing through top electrodes. This suggests that MTJs can be penetrated by γ -ray, and their metal layers cannot shield all γ -rays, especially those with high-energy.

3.3.2. Possible Explanations of Radiation Degradation

Based on the discussion of irradiation penetration mentioned above, it can be concluded that when exposed to γ -rays, MgO barriers should undergo interreaction with

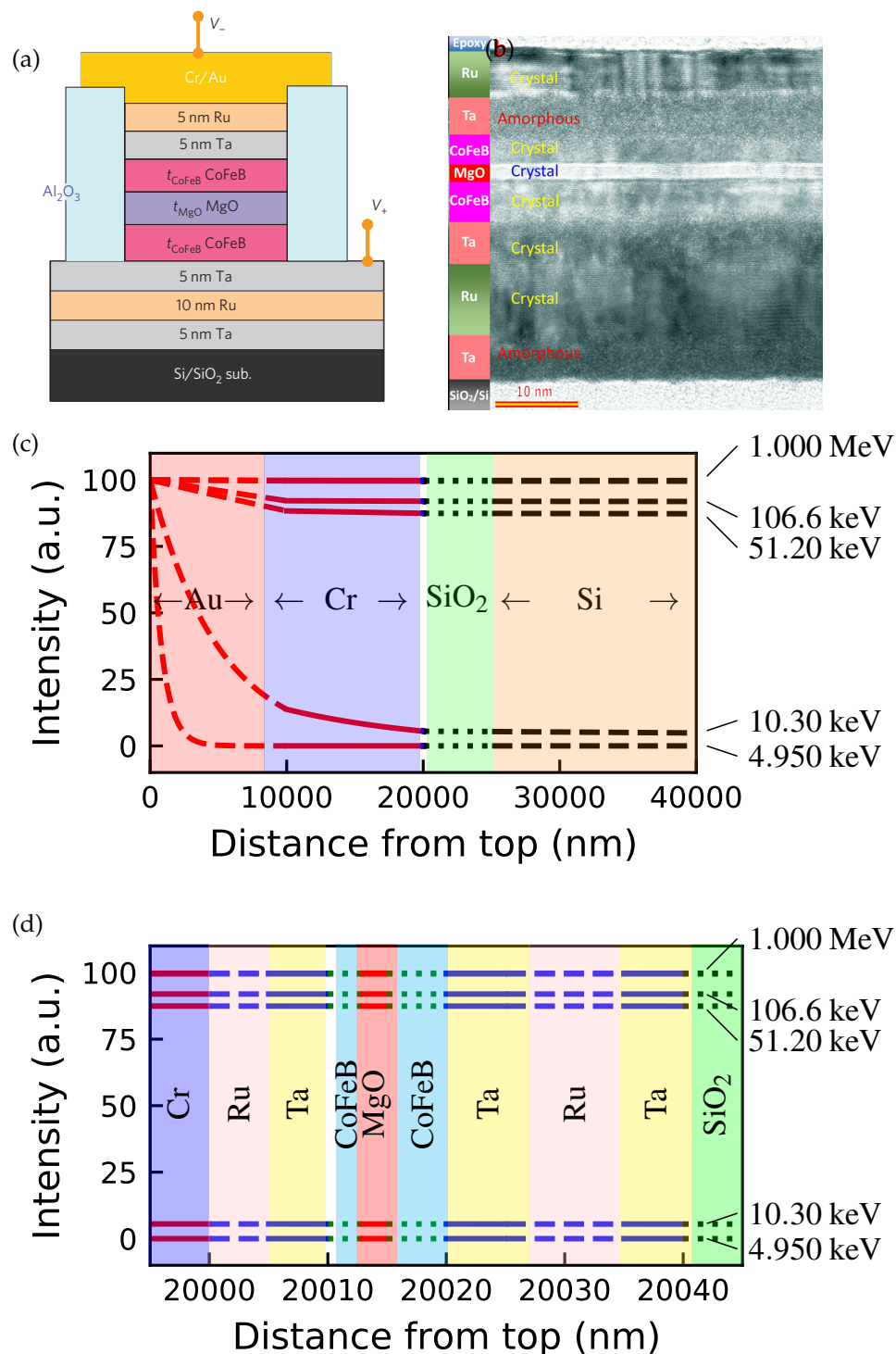


Figure 18. Transmission of electromagnetic radiation through an MTJ device. (a) Structure [181] and (b) HRTEM cross-sectional image [172] of a MTJ device used for penetration calculations of various irradiation. Calculated irradiation intensity through electrodes (c) and sublayers (d), including MgO barriers, under various irradiation energy. The linear attenuation coefficients of the materials were obtained from <https://www.physics.nist.gov>. Reproduced with permission [181] with copyright 2010, Springer Nature. Reproduced with permission [172] with copyright 2016, American Chemical Society.

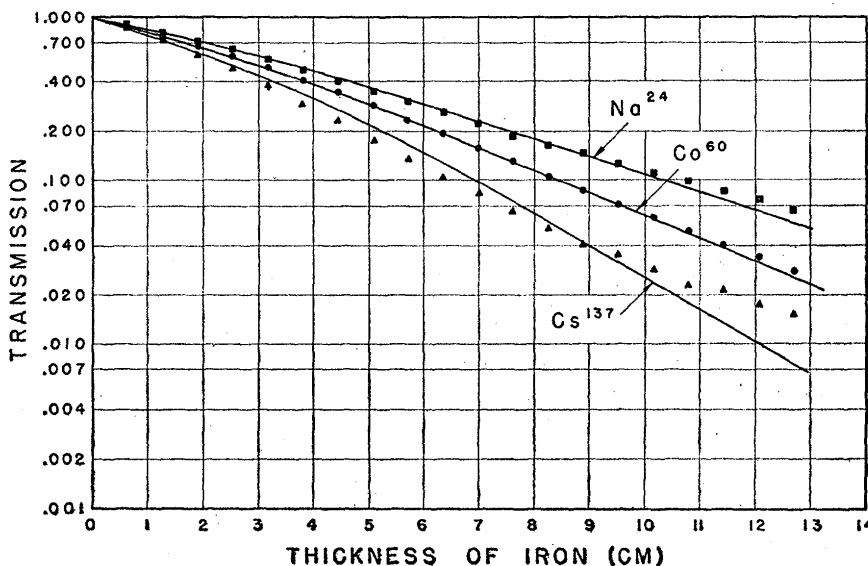


Figure 19. Transmission of γ -radiation through iron. ▲: ^{137}Cs radiation of 0.66 MeV; ●: ^{60}Co radiation of 1.17 MeV and 1.33 MeV; ■: ^{24}Na radiation of 1.38 MeV and 2.76 MeV. Reproduced with permission [118]. Copyright 1953, American Physical Society.

γ -ray, via photoelectric effects, Compton scattering, and electron-positron pair production, discussed in previous sections. These interactions would cause displacement of Mg atoms or O atoms within lattices, resulting in defects or amorphizations of MgO barriers. As a consequence, MTJs would experience γ -ray induced degradation according to the Julliére model.

Figure 20a illustrates the Julliére coherent tunneling in an MTJ with a crystalline MgO barrier and two ferromagnetic layers. The tunneling process involves three kinds of Bloch states with different wave function symmetries existing in the free-/fixed layers, which pass through the MgO barrier. The high MR ratio of the Fe / MgO / Fe sandwich structure primarily depends on the coherent spin-dependent tunneling that occurs in the crystalline MgO(001) tunnel barrier.

Irradiation can have an impact on tunneling. Figure 20b demonstrates the tunneling through a amorphous barrier. When the MgO(001) tunnel barrier becomes amorphous due to irradiation, crystallographic symmetry of the tunnel barrier is lost, Bloch states with various symmetries can couple with the MgO tunneling states, resulting in finite tunneling probabilities. In 3d ferromagnetic metals and alloys, Bloch states with Δ_1 symmetry ($s-p-d$ hybridized states) generally exhibit a large positive spin-polarization P at the Fermi energy E_F , while those with Δ_2 symmetry (d states) tend to have a negative spin-polarization P at E_F [20,184]. All Bloch states in the ferromagnetic free-/fixed layers contribute to the tunneling-current, affecting the net spin-polarization of the ferromagnetic layers and degrading the functionalities of MTJ devices. In other words, after γ irradiation, the momentum of tunneling electrons is no longer conserved due to local disorder scattering. This would destroy the coherence or symmetry of conducting electrons and changes the coherent tunneling process to incoherent tunneling through the displacement of atoms, degrading MTJs. It was experimentally approved that defects of MgO barriers impact polarized tunneling, localized states of spin- and polarized symmetry tunneling across MgO barriers [185]. Electronic properties of MgO grain boundaries in MTJs are symmetry-dependent [186].

In addition, the energy of γ -rays can be transferred to electrons, resulting in an increase in the number of high-energy free spin electrons that interact with the lattices and interfaces. This increase can change the spin-polarization:

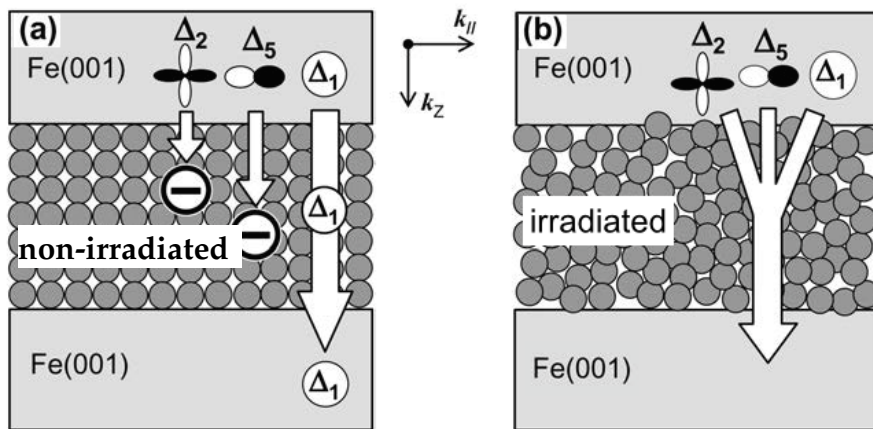


Figure 20. Schematic illustrations of electron tunneling through (a) a crystalline barrier and (b) an irradiated barrier. $\Delta_1 : s - p - d$; $\Delta_2 : d$; $\Delta_5 : p - d$. Re-plotted from Ref. [32]. Reproduced with permission [32] with copyright 2007, IOP Publishing Ltd.

$$P = \frac{N_{\uparrow}(E_F) - N_{\downarrow}(E_F)}{N_{\uparrow}(E_F) + N_{\downarrow}(E_F)} \quad (5)$$

here $N_{\uparrow}(E_F)$ and $N_{\downarrow}(E_F)$ are the density of state at Fermi energy (E_F) for spin-up electrons and spin-down electrons, respectively. γ -ray can change the density of states at E_F , affecting spin- and polarized symmetry tunneling. Additionally, γ -rays can penetrate through the free-/fixed-layers, modifying their electrical and magnetic properties through photoelectric effect and the Compton effects, as well as indirect ionization, which can intermittently or permanently degrade MTJ performances.

According to the Julliére model and the penetration analysis, MgO-based MTJs are expected to degrade under γ -ray irradiation, as reported in some literature. In one word, MTJs should be sensitive to γ -ray irradiation.

3.3.3. Possible Explanations of Tunneling Tolerance

Most research groups have reported that MgO-based MTJs are highly tolerant to γ -ray irradiation and not degraded by γ -ray irradiation at all. There are three possible reasons for this.

One possible explanation of their tolerance to γ -ray is that the unique TMR mechanism of MTJs enables MgO-based MTJs be tolerant. The tunneling mechanism is the most popular explanation. Magnetic properties of MTJs originate from spin than charges, which makes MTJs resistant to radiation. While γ -ray irradiation can amorphize MgO barriers and ferromagnetic fixed- / free-layers, the resulting partial amorphous status of MTJ layers has only *slightly* effects on magnetic characteristics of the fixed- / free-layers [172]. Therefore, the degradation caused by irradiation in MgO-based MTJs is negligible.

Secondly, the degradation of MgO-based MTJs is limited to specific conditions, such as exposure to extremely high doses of radiation, which can result in complete or most partial destruction of crystallographic structures of the MTJ layers and cause MTJs to lose their functionalities. Fortunately, such critical conditions are rarely in γ -ray irradiation, although they can occur in neutron-irradiation and high-energy ion-irradiation. Therefore, the degradation of MTJ under γ -irradiation is expected to be minimal and maybe not to be detected.

Thirdly, many reported measurements have been carried out *ex-situ*. As discussed below, the damages caused by irradiation may diminish over time, and the physical properties of MTJs may be restored when measurements are taken.

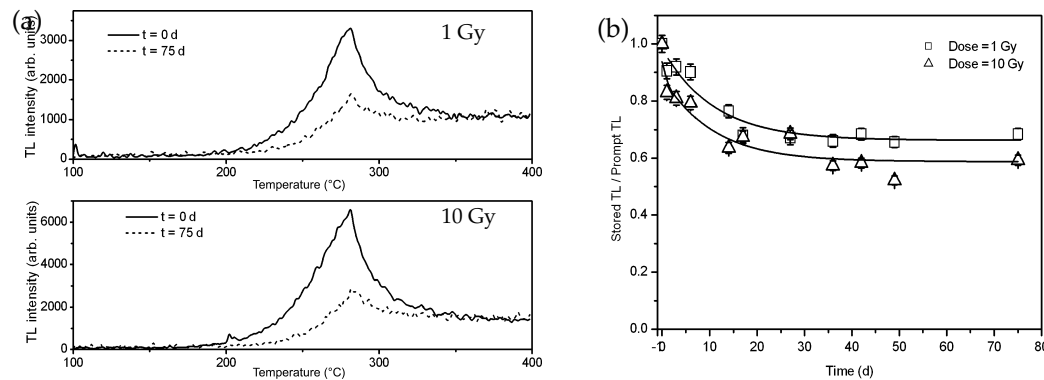


Figure 21. (a) Effect of room temperature restoration of irradiated MgO powders measured for a delay period of 75 days ($t = 75$ d) and without delay ($t = 0$ d). (b) Relative thermoluminescence as a function of restoration time for irradiated MgO. Reproduced with permission [163] with copyright 2009, Taylor & Francis Group.

3.3.4. Possible Explanations for Divergence

It is evident that γ -ray can modify MgO barriers and ferromagnetic layers, and some research groups have reported degradation of MgO-based MTJs as a result. Additionally, a fact that most MTJs cannot operate at high temperatures suggests that MTJs are susceptible to infrared electromagnetic waves, which have lower energy than γ -ray. The temperature-induced degradation indirectly indicates that MTJs should be susceptible to γ -rays with higher energy. However, most research reports have indicated that MgO-based MTJs are tolerant to γ -rays. The divergence among these reports may be explained in the dynamic properties of γ -ray-induced damages, which can account for the divergence among the literature.

Intermittent Defects

Alike high-energy ion irradiation, γ -rays may only induced intermittent defects that do not persist for long time at room temperature and vanish after exposure to irradiation. The excited electrons and ionization can quickly return to the initial state due to thermal motion at room temperature. Figure 13 shows one case where γ -ray changed the physical property (photoconductivity) of MgO, which restored to its initial state after γ -ray irradiation due to thermal motion.

Figure 21 shows another case. The TL intensity of MgO powders irradiated by γ -rays was measured immediately or 75 days after irradiation [163]. The signals induced by γ -ray irradiation diminished over time. Recent calculations have also demonstrated that thermal motion at room temperature can eliminate the impact of γ -irradiation.

Due to the time-dependent dynamic nature of impacts of γ -rays, only *in-situ* measurements can detect the transiently degraded performances of MTJs with excited states. Some studies have reported soft-errors of MgO-based MTJs in *in-situ* measurement under irradiation [167], which were consistent with the assumption of intermittently impacts over time.

Until now, most state-of-the-art measurements have been carried out *ex-situ*, without the presence of γ -rays. Some measurements were performed immediately after γ -ray irradiation, such as within 2 min after removal of irradiation sources [159], or long after irradiation, such as after one year of storage at room temperature before measurements [162]. The impact of irradiation may have diminished prior to measurements. Impact information under γ -rays may decay over time and become undetectable. This may be one explanation for why MgO-based MTJs have been reported to be resistant to γ -irradiation in certain instances.

γ -ray irradiation may only transiently change physical properties of MgO-based MTJ layers during irradiation procedures and do not cause permanent damages. The properties

of MTJ layers can be restored *reversibly* after exposure to γ -ray irradiation, and therefore, MTJs can return to their initial states without irradiation. The intermittent degradation of MgO-based MTJs induced by γ -ray irradiation is not detectable in *ex-situ* measurements.

Irradiation Annealing

Irradiation annealing may eliminate irradiation impacts. High-energy γ -irradiation can produce permanent defects in MgO barriers and ferromagnetic layers, changing their crystallographic structures and physical properties of layers, thereby degrading performances of γ -irradiated MTJs. However, these defects may revert to their initial equilibrium state over time at high temperatures. High dose rate γ -ray irradiation can generate such high temperature in MgO-based MTJs. The irradiation-induced heat can self-anneal MTJs, erasing the effects of γ -irradiation and preventing degradation of γ -irradiated MTJs.

Regrettably, there were few experimental reports on irradiation annealing. The temperature of MgO-barriers and free-/fixed-layers is rarely mentioned in literature, and the time interval between γ -ray irradiation and physical measurements is also unknown. More comprehensive *in-situ* and real-time investigation on the interactions between γ -rays and materials is required.

4. Effects of Lower Energy Irradiation

Electromagnetic waves with wavelengths longer than gamma-rays are commonly known as lower energy waves, such as X-rays, ultraviolet radiation (UV), visible light, infrared radiation, microwaves, and radio waves. These electromagnetic waves have less energy compared to gamma-rays, and are generally classified as non-ionizing radiation, with the exception of X-rays.

4.1. X-ray Irradiation

The energy of X-ray ranges from several tens of electron volts to hundreds of kilo-electron volts. The intensity of X-ray decreases exponentially from surfaces of MTJs, as described by the Beer-Lambert law in Equation 4. X-ray irradiation typically only penetrates a few microns into materials, depending on its energy and material compositions. MgO-based MTJs are typically sandwiched by electric electrodes made of materials such as gold or tantalum. These metal electrodes are usually thick enough to prevent X-ray from penetrating through to MgO barriers and ferromagnetic layers of MTJs. The detailed screening effect can be calculated. Figure 18 shows the calculated penetration intensity of X-ray irradiation with an energy above 4.950 keV (energy of X-ray: 124.8 eV - 124.8 keV). Hard X-ray can fully penetrate MgO-based MTJs with weak absorption, therefor affecting the physical and chemical properties of both MgO barriers as well as ferromagnetic layers. MgO barrier layers should be affected by X-ray irradiation similar to two-dimensional MoS₂ monolayers [113,141]. In this case, the effects of X-ray irradiation on MgO-based MTJs are very similar to those of γ -ray irradiation. These X-ray effects may be also intermittent and only detectable through real-time measurements. Soft X-rays with energies of ten kiloelectron volts or less would be strongly screened by metal electrodes, being prevented penetration through to MgO barriers and ferromagnetic layers of MTJs. Consequently, the effects of soft X-ray irradiation can be disregarded. Up to now, there are few studies of X-ray irradiation on MgO-based MTJs.

4.2. UV-Vis Irradiation

The energy of ultraviolet-visible (UV-Vis) electromagnetic waves ranges from [1eV to several tens electron volts, with a wavelength of 10 – 400 nm]. As shown in Figure 18, UV and visible electromagnetic waves can not penetrate through metal layers to reach ferromagnetic and MgO layers. Additionally, metallic electrodes reflect UV-Vis irradiation, making MgO-based MTJs highly resistant to such irradiation.

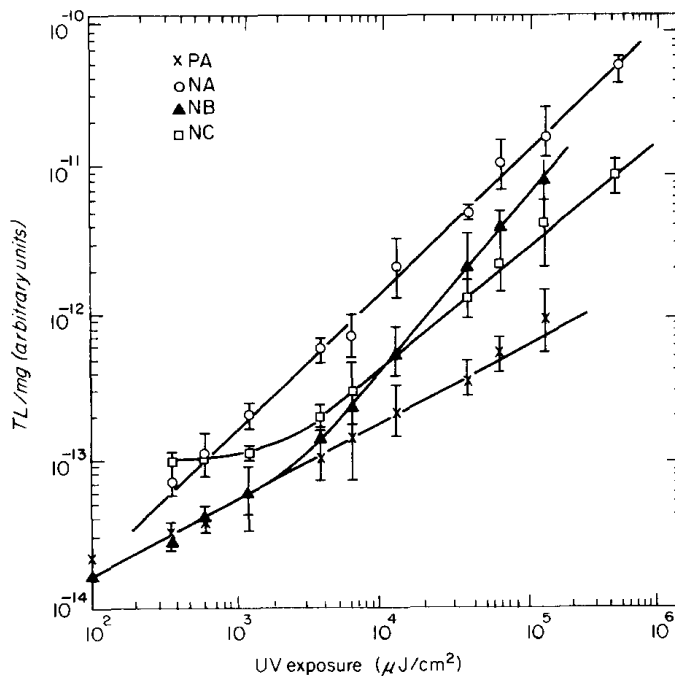


Figure 22. TL response of four MgO crystals as a function of UV exposure at 295 nm. Impurity of PA sample: < 0.026; impurity of NA sample: 0.068; impurity of NB sample: 0.082; impurity of NC sample: < 0.047. Reproduced with permission [187] with copyright 1976, Am. Assoc. Phys. Med.

However, heat produced by UV-Vis irradiation may degrade MgO-based MTJs. Doped MgO materials have been studied as a potential material for UV dosimetry to detect ultraviolet radiation [187,188]. Figure 22 shows thermoluminescent (TL) response of UV-irradiated MgO crystals. Studies have shown that thermoluminescent peaks of doped MgO crystals depend significantly on the dose of ultraviolet irradiation with wavelengths such as 295 nm [187], 289 nm [188], and 249 nm [188]. Even pure MgO crystals are affected by ultraviolet irradiation with wavelengths such as 295 nm UV [187] and 337 nm [189]. Similar behaviors were reported at other ultraviolet wavelengths [188]. These studies demonstrated that UV-irradiation changes microstructures of MgO materials. However, specific physical processes underlying the UV-Vis radiation and MgO materials were not well described in literature. The most likely explanation is that UV-Vis radiation caused an increase in temperature in the MgO materials, leading to their degradation.

It is noteworthy that the changes in TL signals induced by UV-Vis irradiation decreased over time. It was reported that TL intensity of some irradiated crystals restored up to 95 % of initial value after being stored at room temperature for four days [188].

In theory, UV-Vis irradiation should degrade MgO-based MTJs because MgO is sensitive to these electromagnetic waves. However, this degradation should only be intermittent and result from irradiation-induced heating. If heating effects are avoided, MgO-based MTJs should be highly tolerant to UV-Vis irradiation. To date, there is no literature available on the subject of UV-Vis irradiation on MgO-based MTJs.

4.3. Infrared Irradiation and Thermal Annealing

Heat radiation or thermal radiation is a well-known term for infrared irradiation. Pulsed thermal radiation with a long-wavelength of 1 – 20 micron and energy of 1 – 24 eV can be efficiently screened by metallic electrodes. However, continuous thermal radiation, also known as heat, can penetrate MTJ devices during prolonged exposure to high temperatures, resulting in thermal annealing and thermal equilibrium. Thus, infrared irradiation is different somewhat from other types of irradiation.

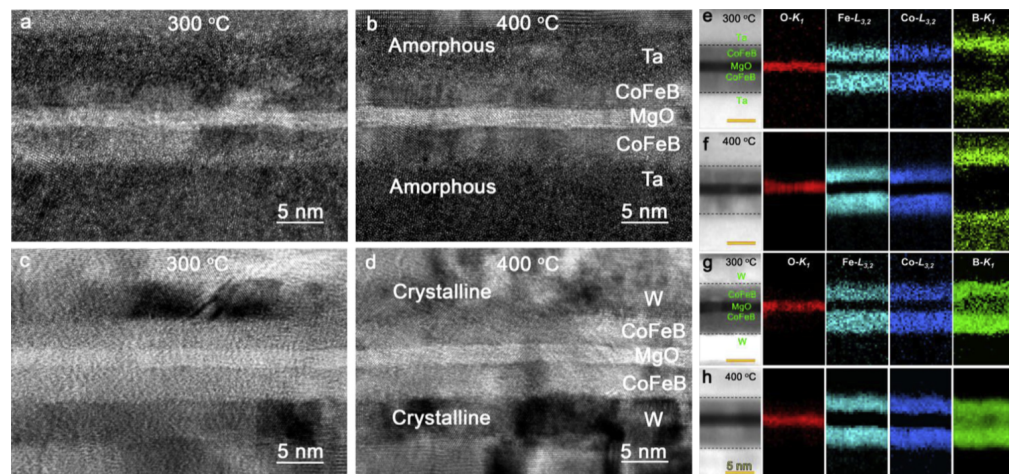


Figure 23. Cross-sectional HRTEM images (*a–d*) and ADF-STEM images and corresponding elemental EELS mappings (*e–h*) using O-K, Fe-L_{3,2}, Co-L_{3,2} and B-K ionization edges taken from the Ta / CoFeB / MgO / CoFeB / Ta MTJ (*a,b,e,f*) and W / CoFeB / MgO / CoFeB MTJ (*c,d,g,h*) at 300 °C (*a,c,e,g*) and 400 °C (*b,d,f,h*). Reproduced with permission [193] with copyright 2018, Elsevier.

There are reports on the annealing effect on MTJ component materials. Nikiforov *et al.* studied the pulse cathodoluminescence (PCL) excitation of MgO nanomaterials with a size of 250 – 500 nm [158]. It was reported that the PCL intensity at 2.0 – 3.5 eV band increased by an order with increasing annealing temperatures, attributed to the relaxation of F-type centers (oxygen vacancies with two captured electrons). Shen *et al.* investigated the impact of thermal annealing on ferromagnetic CoFeB layers [190]. Their investigation indicated that thermal annealing enhanced the crystallization of CoFeB at the interfaces with MgO, affecting the magnetoresistance of MgO-based MTJs. Yuasa *et al.* reviewed the annealing effect on CoFeB electrodes [32], and interested readers are referred to the literature cited therein.

Ikeda *et al.* investigated the effect of thermal annealing on MTJs at high temperatures higher than 500 °C [30]. The MTJs have a structure of in Ta(5) / Ru(10) / Ta(5) / Co₂₀Fe₆₀B₂₀(5) / MgO(2.1) / Co₂₀Fe₆₀B₂₀(4) / Ta(5) / Ru(5) (in nm). It was reported that the annealing process led to the relaxation of residual stress and improvement in the (001) orientation of MgO barriers, resulting in an enhanced TMR ratio.

Wang *et al.* studied both *in-situ* and *ex-situ* measured TMR values at 380 °C [191]. The TMR structure consisted of Si / SiO₂ / Ta(7) / Ru(20) / Ta(7) / CoFe(2) / IrMn(15) / CoFe(2) / Ru(1.7) / CoFeB(3) / MgO(1.5 - 3) / CoFeB(3) / Ta(8) / Ru(10), with the numbers indicating the layer thicknesses in nanometers. It was found that the amorphous CoFeB layers underwent crystallization, and the quality of MgO barriers' crystallinity improved in less than 10 min annealing, resulting in a TMR value larger than 200 %. The crystallization was further experimentally confirmed through their HRTEM work [172].

Liu *et al.* investigated the thermal stability of MTJs with MgO barriers at temperatures up to 500 °C [192]. The MTJs consisted of Ta(30) / [Co₅₀Fe₅₀]₃ / IrMn(15) / [Co₅₀Fe₅₀]₂ / Ru(0.8) / [Co₄₀Fe₄₀B₂₀]₃ / MgO(1.2) / [Co₄₀Fe₄₀B₂₀]₃ / Ta(10) / Ru(5). The study observed irreversible loss of magnetoresistance at high temperatures.

Typically, thermal annealing (using infrared radiation) has a positive benefit on the crystallization of MgO barriers, which enhances the performances of MTJs. However, thermal annealing also accelerates interface diffusion between MgO barriers and ferromagnetic layers, leading to degradation of MTJ performances [194]. Xu *et al.* employed transmission electron microscopy and electron energy loss spectroscopy to investigate the microstructures of MgO-CoFeB interfaces of MTJs [193]. Figure 23 shows HRTEM images, STEM images, and EELS mapping of the interfaces after thermal annealing. Thermal annealing indeed crystallized MTJ layers, as shown by the HRTEM images, and caused

boron diffusion. Boron diffusion led to the growth of CoFe nanocrystals from CoFeB layers under annealing, while the crystallization did not significantly affect the MR properties. Instead, the MR ratio was predominantly determined by grain boundary transport caused by boron distribution. If boron diffused to metallic underlayers from the inside to the outside (as shown in Figure 23e-f), the MR ratio would be improved. Conversely, annealing may result in boron diffusing into grain boundaries of MgO barriers from the outside to the inside (shown in Figure 23g-h), leading to a decrease in the MR ratio. The interfacial properties of MTJs regulated the diffusion of boron and affected the effect of thermal annealing. Thus, the effect of thermal irradiation on MTJ devices depends on annealing temperature, duration, and structures of MTJs. Thermal irradiation can either benefit or degrade MTJs' performances.

It is important to notice that irradiation other than infrared irradiation can also produce heat, particularly at high-dose rates, which can lead to an increase in temperatures of MTJs and produce similar annealing effects. Under such circumstances, high-energy irradiation, such as γ -ray and hard X-ray irradiation, may cause additional annealing effects. To study the effects of irradiation, it is crucial to investigate MTJs at constant temperatures or monitor the internal temperatures of MTJs, particularly the temperatures of MgO and ferromagnetic layers.

4.4. Microwave Irradiation

The penetration depth of microwaves on conductive metal surfaces is typically less than one micron [195]. Therefore, metallic electrodes of MTJs can highly reflect microwaves. In other words, microwaves should not penetrate through electrodes to irradiate MgO barriers and ferromagnetic layers. Therefore, the microwave irradiation effect would be ignored, and microwave irradiation should not have any significant impact on the performance of MTJs.

Although microwave irradiation is not expected to penetrate through electrodes of MTJs to affect MgO barriers and ferromagnetic layers, it can cause a significant increase in temperature of metal layers. Research has shown that microwave irradiation can produce a high temperature of up to 500 °C in Au films in less than 10 seconds [196]. Therefore, microwave irradiation can generate a high temperature locally in ferromagnetic free-layers of MTJs, which can have a significant impact on the performance of MTJs.

Up to now, there are limited reports on the impact of microwave irradiation on MgO-based MTJs. Some groups investigated the behavior of MgO-based MTJs under microwave irradiation [95]. Unfortunately, it was not stated whether the MgO-based MTJs were damaged under microwave irradiation.

4.5. Radio Frequency Electromagnetic Irradiation

Radio-frequency (RF) electromagnetic radiation can be shielded by conductive or magnetic materials, which is known as RF shielding. Since MTJs have metal electrodes, electrodes can block RF radiation and therefore MTJs should not be affected. The theoretical calculation shown in Figure 18 also predicts that electromagnetic waves with energy lower than four kiloelectron volts would not penetrate through electrodes of MTJs. As listed in Table 1, energy of radio-frequency irradiation is typically less than a few milli-electronvolts, so RF irradiation should be totally shielded and not affect MTJ performance.

Similar to microwaves, RF irradiation can also induce heating in metals, leading to high temperatures locally on MTJ electrodes. However, the induced temperature is expected to be low due to extremely low energy of IR radiation.

Therefore, effects of radio-frequency and other electromagnetic irradiation with longer wavelength can be ignored. MgO-based MTJs should be highly tolerant to these irradiation.

5. Outlook

MgO-based MTJs are promising for various applications, such as MRAM in quantum computers, logic gates, ultra-sensitive sensors, and energy harvesting and storage. These

devices can be utilized in space technology, and therefore, the impact of radiation is crucial. With advancements in super-large-scale integration (SLSI) technology for central processing units (CPUs) and graphics processing units (GPUs) and programming languages like open-source Python programming language as well as professional packages / libraries for programming languages, it is possible to simulate complex interactions between irradiation and MTJ components at the atomic level. Dynamic simulations at atomic level can be employed to investigate individual atomic motion and nanoscale displacement under irradiation, to calculate MR, providing insights into the dynamic behavior of atoms during irradiation. Additionally, the development of artificial intelligence (AI), including machine learning and deep learning, makes it possible to collect most research data on irradiation of MgO-based MTJs and systematically analyze irradiation impacts. Various parameters, such as irradiation energy, irradiation duration, dose, and dose rate, can be simulated investigated and compared with experimental data to understand electromagnetic-material interaction. Safe operation of MgO-based MTJs can be predicted in various irradiation environments.

6. Conclusions

The effects of irradiation on MgO-based magnetic tunnel junctions have been reviewed and analyzed in various irradiation environments, including high-energy cosmic radiation, gamma-ray, X-ray, UV-vis, infrared irradiation, microwave irradiation, radio frequency, and long wavelength electromagnetic irradiation. The examination considered both material properties and device performance. In general, cosmic radiations (including ions and protons) can damage MTJs due to permanent atom displacements in MTJ layers. While some groups have reported that γ -ray irradiation degrades the performance of MgO-based MTJs, the majority of scientists have claimed that MgO-based MTJs are tolerant to γ -ray without significant degradation in their performance. The impact of hard X-ray irradiation is comparable to that of γ -ray irradiation. Soft X-ray, UV-vis, infrared, and microwave irradiation can be screened or shielded by metal electrodes of MTJs, and these types of electromagnetic irradiation should not significantly affect MTJ devices. Nonetheless, these types of irradiation may induce heat or annealing, especially for infrared and microwave irradiation, which can affect MRJ performances by causing crystallization of MgO barriers and ferromagnetic layers as well as interfacial diffusion. There is no strong evidence that the present MgO-based MTJ devices are susceptible to irradiation. The effects of irradiation on MgO-based MTJs are discussed from electromagnetic penetration, Julliére model, TMR mechanism, and annealing perspectives, to explore the physics behind these reported experimental data. Further *in-situ* and real-time investigations are necessary to fully understand the irradiation tolerance of MgO-based MTJ devices under various electromagnetic irradiation.

Author Contributions: Conceptualization, Q. P. and Y. L.; writing—original draft preparation, D. S., Q. P., F. C., and Y. L.; writing—review and editing, D. S., Q. P., F. C., and Y. L.; reference and formatting: J. H. and Y. L.; visualization, K. S. and Y. L. All authors have read and agreed to the published version of the manuscript.

Acknowledgments: Y. L. is partially supported by DOE DE-FE0031906. D. S. acknowledge the support of U. S. Army Research Laboratory grant USARMY-W911NF-19-2-0222. Q. P. would like to acknowledge the support provided by the Deanship of Scientific Research (DSR) at King Fahd University of Petroleum & Minerals (KFUPM) through project DF201020. The views and conclusions presented in this document are those of the authors and do not be interpreted as representing the official policies, either expressed or implied, of the Army Research Laboratory or the U. S. Government. The U. S. Government is authorized to reproduce and distribute reprints for government purposes notwithstanding any copyright notation contained herein.

Conflicts of Interest: The authors declare no conflict of interest.

Abbreviations

The following abbreviations are used in this manuscript:

ADC	analog-to-digital converter	1178
AMR	anisotropic magnetoresistance	1179
CMOS	complementary metal-oxide-semiconductor	
DC	direct-current	
DRAM	dynamic random-access memory	
GMR	giant magnetoresistance	
HDD	hard disk drive	
MOS	metal oxide sensor	
MR	magnetoresistance	
MRAM	magnetic random-access memory	
MTJ	magnetic tunnel junction	1180
PV	photovoltaic	
RAM	random-access memory	
RF	radio-frequency	
RT	room-temperature	
SEM	scanning electron microscopy	
SRAM	static random-access memory	
TE	thermoelectric	
TEM	transmission electron microscopy	
TMR	tunnel magnetoresistance	

References

- Wolf, S.A.; Awschalom, D.D.; Buhrman, R.A.; Daughton, J.M.; von Molnár, S.; Roukes, M.L.; Chtchelkanova, A.Y.; Treger, D.M. Spintronics: A spin-based electronics vision for the future. *Science* **2001**, *294*, 1488–1495. doi:10.1126/science.1065389.
- Yuasa, S.; Nagahama, T.; Fukushima, A.; Suzuki, Y.; Ando, K. Giant room-temperature magnetoresistance in single-crystal Fe/MgO/Fe magnetic tunnel junctions. *Nat. Mater.* **2004**, *3*, 868–871. doi:10.1038/nmat1257.
- Djayaprawira, D.D.; Tsunekawa, K.; Nagai, M.; Maehara, H.; Yamagata, S.; Watanabe, N.; Yuasa, S.; Suzuki, Y.; Ando, K. 230 % room-temperature magnetoresistance in CoFeB/MgO/CoFeB magnetic tunnel junctions. *Appl. Phys. Lett.* **2005**, *86*, 092502. doi:10.1063/1.1871344.
- Newman, A.; Khatiwada, S.; Neupane, S.; Seifu, D. Nanowires of Fe/multi-walled carbon nanotubes and nanometric thin films of Fe/MgO. *J. Appl. Phys.* **2015**, *117*, 144302. doi:10.1063/1.4917051.
- Bowen, M.; Cros, V.; Petroff, F.; Fert, A.; Martínez Boubeta, C.; Costa-Krämer, J.L.; Anguita, J.V.; Cebollada, A.; Briones, F.; de Teresa, J.M.; et al. Large magnetoresistance in Fe/MgO/FeCo(001) epitaxial tunnel junctions on GaAs(001). *Appl. Phys. Lett.* **2001**, *79*, 1655–1657. doi:10.1063/1.1404125.
- Bland, J.A.C.; Heinrich, B. *Ultrathin Magnetic Structures I: An Introduction to the Electronic, Magnetic and Structural Properties*; Springer Science & Business Media, 1994.
- Gallagher, W.; Parkin, S. Development of the magnetic tunnel junction MRAM at IBM: From first junctions to a 16-Mb MRAM demonstrator chip. *IBM J. Res. Dev.* **2006**, *50*, 5–23. doi:10.1147/rd.501.0005.
- Seifu, D. Nanowires of Fe/MgO/Fe encapsulated in carbon nanotubes. In *Nanowires-Synthesis, Properties and Applications*; IntechOpen, 2018.
- Thomson, W. On the electro-dynamic qualities of metals: Effects of magnetization on the electric conductivity of nickel and of iron. *Proc. R. Soc. London* **1856**, *8*, 546–550. doi:10.1098/rspl.1856.0144.
- Nickel, J. Magnetoresistance overview. *HP Labs Technical Reports: HPL-95-60* **1995**.
- McGuire, T.; Potter, R. Anisotropic magnetoresistance in ferromagnetic 3d alloys. *IEEE Trans. Magn.* **1975**, *11*, 1018–1038. doi:10.1109/TMAG.1975.1058782.
- Baibich, M.N.; Broto, J.M.; Fert, A.; Van Dau, F.N.; Petroff, F.; Etienne, P.; Creuzet, G.; Friederich, A.; Chazelas, J. Giant magnetoresistance of (001)Fe/(001)Cr magnetic superlattices. *Phys. Rev. Lett.* **1988**, *61*, 2472–2475. doi:10.1103/PhysRevLett.61.2472.
- Binasch, G.; Grünberg, P.; Saurenbach, F.; Zinn, W. Enhanced magnetoresistance in layered magnetic structures with antiferromagnetic interlayer exchange. *Phys. Rev. B* **1989**, *39*, 4828–4830. doi:10.1103/PhysRevB.39.4828.
- Camley, R.E.; Barnaś, J. Theory of giant magnetoresistance effects in magnetic layered structures with antiferromagnetic coupling. *Phys. Rev. Lett.* **1989**, *63*, 664–667. doi:10.1103/PhysRevLett.63.664.
- Yuasa, S. Giant tunneling magnetoresistance in MgO-based magnetic tunnel junctions. *J. Phys. Soc. Jpn.* **2008**, *77*, 031001. doi:10.1143/JPSJ.77.031001.
- Zhu, J.G.; Park, C. Magnetic tunnel junctions. *Materials Today* **2006**, *9*, 36–45. doi:10.1016/S1369-7021(06)71693-5.
- Chappert, C.; Fert, A.; Van Dau, F.N. The emergence of spin electronics in data storage. *Nat. Mater.* **2007**, *6*, 813–823. doi:10.1038/nmat2024.
- Jullière, M. Tunneling between ferromagnetic films. *Phys. Lett. A* **1975**, *54*, 225–226. doi:10.1016/0375-9601(75)90174-7.

19. Miyazaki, T.; Tezuka, N. Giant magnetic tunneling effect in Fe/Al₂O₃/Fe junction. *J. Magn. Magn. Mater.* **1995**, *139*, L231 – L234. doi:10.1016/0304-8853(95)90001-2. 1217
1218
20. Yuasa, S.; Nagahama, T.; Suzuki, Y. Spin-polarized resonant tunneling in magnetic tunnel junctions. *Science* **2002**, *297*, 234 – 237. doi:10.1126/science.1071300. 1219
1220
21. Wang, D.; Nordman, C.; Daughton, J.; Qian, Z.; Fink, J. 70 % TMR at room temperature for SDT sandwich junctions with CoFeB as free and reference layers. *IEEE Trans. Magn.* **2004**, *40*, 2269 – 2271. doi:10.1109/TMAG.2004.830219. 1221
1222
22. Yuasa, S., Introduction to magnetic random-access memory; Wiley-Blackwell, 2016; chapter Magnetic Properties of Materials for MRAM, pp. 29 – 54. doi:10.1002/9781119079415. 1223
1224
23. Moodera, J.S.; Kinder, L.R. Ferromagnetic-insulator-ferromagnetic tunneling: Spin-dependent tunneling and large magnetoresistance in trilayer junctions (invited). *J. Appl. Phys.* **1996**, *79*, 4724 – 4729. doi:10.1063/1.361653. 1225
1226
24. Faure-Vincent, J.; Tiusan, C.; Jouguet, E.; Canet, F.; Sajieddine, M.; Bellouard, C.; Popova, E.; Hehn, M.; Montaigne, F.; Schuhl, A. High tunnel magnetoresistance in epitaxial Fe/MgO/Fe tunnel junctions. *Appl. Phys. Lett.* **2003**, *82*, 4507 – 4509. doi:10.1063/1.1586785. 1227
1228
25. Yuasa, S.; Fukushima, A.; Nagahama, T.; Ando, K.; Suzuki, Y. High tunnel magnetoresistance at room temperature in fully epitaxial Fe/MgO/Fe tunnel junctions due to coherent spin-polarized tunneling. *Jpn. J. Appl. Phys.* **2004**, *43*, L588. doi:10.1143/JJAP.43.L588. 1229
1230
26. Parkin, S.S.P.; Kaiser, C.; Panchula, A.; Rice, P.M.; Hughes, B.; Samant, M.; Yang, S.H. Giant tunnelling magnetoresistance at room temperature with MgO (100) tunnel barriers. *Nat. Mater.* **2004**, *3*, 862 – 867. doi:10.1038/nmat1256. 1233
1234
27. Ikeda, S.; Hayakawa, J.; Lee, Y.M.; Sasaki, R.; Meguro, T.; Matsukura, F.; Ohno, H. Dependence of tunnel magnetoresistance in MgO based magnetic tunnel junctions on Ar pressure during MgO sputtering. *Jpn. J. Appl. Phys.* **2005**, *44*, L1442. doi:10.1143/JJAP.44.L1442. 1235
1236
28. Yuasa, S.; Fukushima, A.; Kubota, H.; Suzuki, Y.; Ando, K. Giant tunneling magnetoresistance up to 410 % at room temperature in fully epitaxial Co/MgO/Co magnetic tunnel junctions with bcc Co(001) electrodes. *Appl. Phys. Lett.* **2006**, *89*, 042505. doi:10.1063/1.2236268. 1238
1239
29. Lee, Y.M.; Hayakawa, J.; Ikeda, S.; Matsukura, F.; Ohno, H. Effect of electrode composition on the tunnel magnetoresistance of pseudo-spin-valve magnetic tunnel junction with a MgO tunnel barrier. *Appl. Phys. Lett.* **2007**, *90*, 212507. doi:10.1063/1.2742576. 1241
1242
30. Ikeda, S.; Hayakawa, J.; Ashizawa, Y.; Lee, Y.M.; Miura, K.; Hasegawa, H.; Tsunoda, M.; Matsukura, F.; Ohno, H. Tunnel magnetoresistance of 604 % at 300 K by suppression of Ta diffusion in CoFeB/MgO/CoFeB pseudo-spin-valves annealed at high temperature. *Appl. Phys. Lett.* **2008**, *93*, 082508. doi:10.1063/1.2976435. 1243
1244
31. Ikeda, S.; Hayakawa, J.; Ashizawa, Y.; Lee, Y.; Miura, K.; Hasegawa, H.; Tsunoda, M.; Matsukura, F.; Ohno, H. Tunnel magnetoresistance of 604 % at 300 K by suppression of Ta diffusion in CoFeB/MgO/CoFeB pseudo-spin-valves annealed at high temperature. *Appl. Phys. Lett.* **2008**, *93*, 082508. doi:10.1063/1.2976435. 1245
1246
32. Yuasa, S.; Djayaprawira, D.D. Giant tunnel magnetoresistance in magnetic tunnel junctions with a crystalline MgO(001) barrier. *J. Phys. D: Appl. Phys.* **2007**, *40*, R337. doi:10.1088/0022-3727/40/21/R01. 1249
1250
33. Åkerman, J. Toward a Universal Memory. *Science* **2005**, *308*, 508 – 510. doi:10.1126/science.1110549. 1251
34. Mao, S.; Chen, Y.; Liu, F.; Chen, X.; Xu, B.; Lu, P.; Patwari, M.; Xi, H.; Chang, C.; Miller, B.; et al. Commercial TMR heads for hard disk drives: characterization and extendibility at 300 Gbit/in². *IEEE Trans. Magn.* **2006**, *42*, 97 – 102. doi:10.1109/TMAG.2005.861788. 1252
1253
35. Puebla, J.; Kim, J.; Kondou, K.; Otani, Y. Spintronic devices for energy-efficient data storage and energy harvesting. *Commun. Mater.* **2020**, *1*, 24. doi:10.1038/s43246-020-0022-5. 1255
1256
36. Hosomi, M.; Yamagishi, H.; Yamamoto, T.; Bessho, K.; Higo, Y.; Yamane, K.; Yamada, H.; Shoji, M.; Hachino, H.; Fukumoto, C.; et al. A novel nonvolatile memory with spin torque transfer magnetization switching: spin-RAM. IEEE International Electron Devices Meeting, 2005. IEDM Technical Digest., 2005, pp. 459 – 462. doi:10.1109/IEDM.2005.1609379. 1257
1258
37. Ho, M.; Tsang, C.; Fontana, R.E.; Parkin, S.; Carey, K.; Pan, T.; MacDonald, S.; Arnett, P.; Moore, J. Study of magnetic tunnel junction read sensors. *IEEE Trans. Magn.* **2001**, *37*, 1691 – 1694. doi:10.1109/20.950939. 1259
1260
38. Mao, S.; Nowak, J.; Song, D.; Kolbo, P.; Wang, L.; Linville, E.; Saunders, D.; Murdock, E.; Ryan, P. Spin tunneling heads above 20 Gb/in². *IEEE Trans. Magn.* **2002**, *38*, 78 – 83. doi:10.1109/TMAG.2002.988915. 1262
1263
39. Araki, S.; Sato, K.; Kagami, T.; Saruki, S.; Uesugi, T.; Kasahara, N.; Kuwashima, T.; Ohta, N.; Sun, J.; Nagai, K.; et al. Fabrication and electrical properties of lapped type of TMR heads for ~ 50 Gb/in² and beyond. *IEEE Trans. Magn.* **2002**, *38*, 72 – 77. doi:10.1109/TMAG.2002.988914. 1264
1265
40. Mao, S.; Linville, E.; Nowak, J.; Zhang, Z.; Chen, S.; Karr, B.; Anderson, P.; Ostrowski, M.; Boonstra, T.; Cho, H.; et al. Tunneling magnetoresistive heads beyond 150 Gb/in². *IEEE Trans. Magn.* **2004**, *40*, 307 – 312. doi:10.1109/TMAG.2003.821167. 1267
1268
41. Kagami, T.; Kuwashima, T.; Miura, S.; Uesugi, T.; Barada, K.; Ohta, N.; Kasahara, N.; Sato, K.; Kanaya, T.; Kiyono, H.; et al. A performance study of next generation's TMR heads beyond 200 Gb/in². *IEEE Trans. Magn.* **2006**, *42*, 93 – 96. doi:10.1109/TMAG.2005.861796. 1269
1270
42. Horiguchi, F. Multi-value magnetic random access memory with stacked tunnel magnetoresistance (TMR) elements, 2006. US Patent 7,042,753. 1272
1273
43. Tehrani, S.; Chen, E.; Durlam, M.; DeHerrera, M.; Slaughter, J.M.; Shi, J.; Kerszykowski, G. High density submicron magnetoresistive random access memory (invited). *J. Appl. Phys.* **1999**, *85*, 5822 – 5827. doi:10.1063/1.369931. 1274
1275

44. Parkin, S.S.P.; Roche, K.P.; Samant, M.G.; Rice, P.M.; Beyers, R.B.; Scheuerlein, R.E.; O'Sullivan, E.J.; Brown, S.L.; Bucchignano, J.; Abraham, D.W.; et al. Exchange-biased magnetic tunnel junctions and application to nonvolatile magnetic random access memory (invited). *J. Appl. Phys.* **1999**, *85*, 5828–5833. doi:10.1063/1.369932. 1277
45. Tehrani, S.; Slaughter, J.; Chen, E.; Durlam, M.; Shi, J.; DeHerren, M. Progress and outlook for MRAM technology. *IEEE Trans. Magn.* **1999**, *35*, 2814–2819. doi:10.1109/20.800991. 1279
46. Engel, B.; Rizzo, N.; Janesky, J.; Slaughter, J.M.; Dave, R.; DeHerrera, M.; Durlam, M.; Tehrani, S. The science and technology of magnetoresistive tunneling memory. *IEEE Trans. Nanotechno.* **2002**, *1*, 32–38. doi:10.1109/TNANO.2002.1005424. 1281
47. Katti, R. Giant magnetoresistive random-access memories based on current-in-plane devices. *Proc. IEEE* **2003**, *91*, 687–702. doi:10.1109/JPROC.2003.811805. 1283
48. Tehrani, S.; Slaughter, J.M.; DeHerrera, M.; Engel, B.; Rizzo, N.; Salter, J.; Durlam, M.; Dave, R.; Janesky, J.; Butcher, B.; et al. Magnetoresistive random access memory using magnetic tunnel junctions. *Proc. IEEE* **2003**, *91*, 703–714. doi:10.1109/JPROC.2003.811804. 1285
49. Engel, B.; Åkerman, J.; Butcher, B.; Dave, R.; DeHerrera, M.; Durlam, M.; Gryniewich, G.; Janesky, J.; Pietambaram, S.; Rizzo, N.; et al. A 4-Mb toggle MRAM based on a novel bit and switching method. *IEEE Trans. Magn.* **2005**, *41*, 132–136. doi:10.1109/TMAG.2004.840847. 1288
50. Zhu, J.G. Magnetoresistive random access memory: The path to competitiveness and scalability. *Proc. IEEE* **2008**, *96*, 1786–1798. doi:10.1109/JPROC.2008.2004313. 1291
51. Dave, R.; Steiner, G.; Slaughter, J.; Sun, J.; Craig, B.; Pietambaram, S.; Smith, K.; Gryniewich, G.; DeHerrera, M.; Åkerman, J.; et al. MgO-based tunnel junction material for high-speed toggle magnetic random access memory. *IEEE Trans. Magn.* **2006**, *42*, 1935–1939. doi:10.1109/TMAG.2006.877743. 1294
52. Gallagher, W.J.; Parkin, S.S.P.; Lu, Y.; Bian, X.P.; Marley, A.; Roche, K.P.; Altman, R.A.; Rishton, S.A.; Jahnes, C.; Shaw, T.M.; et al. Microstructured magnetic tunnel junctions (invited). *J. Appl. Phys.* **1997**, *81*, 3741–3746. doi:10.1063/1.364744. 1296
53. Gerardin, S.; Paccagnella, A. Present and future non-volatile memories for space. *IEEE Trans. Nucl. Sci.* **2010**, *57*, 3016–3039. doi:10.1109/TNS.2010.2084101. 1299
54. Jiang, Y.; Lv, Y.; Jamali, M.; Wang, J.P. Spin analog-to-digital convertor using magnetic tunnel junction and spin Hall effect. *IEEE Electron Device Lett.* **2015**, *36*, 511–513. doi:10.1109/LED.2015.2416689. 1301
55. Maciel, N.; Marques, E.; Naviner, L.; Cai, H. Magnetic tunnel junction-based analog-to-digital converter using spin orbit torque mechanism. 2020 27th IEEE International Conference on Electronics, Circuits and Systems (ICECS), 2020, pp. 1–4. doi:10.1109/ICECS49266.2020.9294780. 1303
56. Wu, Y.a.; Naviner, L.; Cai, H. Hybrid MTJ-CMOS integration for Sigma-Delta ADC. 2021 IEEE/ACM International Symposium on Nanoscale Architectures (NANOARCH), 2021, pp. 1–5. doi:10.1109/NANOARCH53687.2021.9642236. 1305
57. Paz, E.; Serrano-Guisan, S.; Ferreira, R.; Freitas, P.P. Room temperature direct detection of low frequency magnetic fields in the 100 pT/Hz^{0.5} range using large arrays of magnetic tunnel junctions. *J. Appl. Phys.* **2014**, *115*, 17E501. doi:10.1063/1.4859036. 1307
58. Ferreira, R.; Wisnioski, P.; Freitas, P.P.; Langer, J.; Ocker, B.; Maass, W. Tuning of MgO barrier magnetic tunnel junction bias current for picotesla magnetic field detection. *J. Appl. Phys.* **2006**, *99*, 08K706. doi:10.1063/1.2173636. 1310
59. Fan, X.; Cao, R.; Moriyama, T.; Wang, W.; Zhang, H.W.; Xiao, J.Q. Magnetic tunnel junction based microwave detector. *Appl. Phys. Lett.* **2009**, *95*, 122501. doi:10.1063/1.3231874. 1311
60. Fan, X.; Chen, Y.; Bi, C.; Xie, Y.; Kolodzey, J.; Wilson, J.D.; Simons, R.N.; Zhang, H.; Xiao, J.Q. Magnetic tunnel junction-based on-chip microwave phase and spectrum analyzer. 2014 IEEE MTT-S International Microwave Symposium (IMS2014), 2014, pp. 1–4. doi:10.1109/MWSYM.2014.6848560. 1314
61. Sengupta, A.; Liyanagedera, C.M.; Jung, B.; Roy, K. Magnetic tunnel junction as an on-chip Temperature Sensor. *Sci. Rep.* **2017**, *7*, 11764. doi:10.1038/s41598-017-11476-7. 1316
62. Bauer, G.E.W.; Saitoh, E.; van Wees, B.J. Spin caloritronics. *Nat. Mater.* **2012**, *11*, 391–399. doi:10.1038/nmat3301. 1318
63. Otani, Y.; Shiraishi, M.; Oiwa, A.; Saitoh, E.; Murakami, S. Spin conversion on the nanoscale. *Nat. Phys.* **2017**, *13*, 829–832. doi:10.1038/nphys4192. 1319
64. BCS, I. Waste Heat Recovery: Technology and Opportunities in U.S. Industry. Technical report, 2008. 1321
65. Dresselhaus, M.; Chen, G.; Tang, M.Y.; Yang, R.G.; Lee, H.; Wang, D.Z.; Ren, Z.F.; Fleurial, J.P.; Gogna, P. New Directions for Low-Dimensional Thermoelectric Materials. *Adv. Mater.* **2007**, *19*, 1043–1053. doi:10.1002/adma.200600527. 1322
66. Poudel, B.; Hao, Q.; Ma, Y.; Lan, Y.; Minnich, A.; Yu, B.; Yan, X.; Wang, D.; Muto, A.; Vashaee, D.; et al. High-thermoelectric performance of nanostructured bismuth antimony telluride bulk alloys. *Science* **2008**, *320*, 634–638. doi:10.1126/science.1156446. 1324
67. Lan, Y.C.; Wang, D.Z.; Chen, G.; Ren, Z.F. Diffusion of nickel and tin in *p*-type (Bi,Sb)₂Te₃ and *n*-type Bi₂(Te,Se)₃ thermoelectric materials. *Appl. Phys. Lett.* **2008**, *92*, 101910/1–101910/3. doi:10.1063/1.2896310. 1326
68. Lan, Y.; Poudel, B.; Ma, Y.; Wang, D.; Dresselhaus, M.S.; Chen, G.; Ren, Z. Structure study of bulk nanograined thermoelectric bismuth antimony telluride **2009**, *9*, 1419–1422. doi:10.1021/nl803235n. 1328
69. Lan, Y.; Minnich, A.J.; Chen, G.; Ren, Z. Enhancement of thermoelectric figure-of-merit by a bulk nanostructuring approach. *Adv. Func. Mater.* **2010**, *20*, 357–376. doi:10.1002/adfm.200901512. 1331
70. Liu, W.; Yan, X.; Chen, G.; Ren, Z. Recent advances in thermoelectric nanocomposites. *Nano Energy* **2012**, *1*, 42–56. doi:<https://doi.org/10.1016/j.nanoen.2011.10.001>. 1332

71. Ren, Z.; Lan, Y.; Zhang, Q., Eds. *Advanced Thermoelectrics: Materials, Contacts, Modules, and Systems*; CRC Press, Taylor & Francis Group: Boca Raton, FL, 2017. [1334](#)
72. Bao, X.; Hou, S.; Wu, Z.; Wang, X.; Yin, L.; Liu, Y.; He, H.; Duan, S.; Wang, B.; Mao, J.; et al. Mechanical properties of thermoelectric generators. *J. Mater. Sci. Technol.* **2023**, *148*, 64–74. doi:10.1016/j.jmst.2022.10.081. [1335](#)
73. Liu, Z.; Gao, W.; Guo, F.; Cai, W.; Zhang, Q.; Sui, J. Challenges for Thermoelectric Power Generation: From a Material Perspective. *Materials Lab* **2022**, *1*, 220003–1–220003–12. doi:10.54227/mlab.20220003. [1336](#)
74. Mao, J.; Liu, Z.; Zhou, J.; Zhu, H.; Zhang, Q.; Chen, G.; Ren, Z. Advances in thermoelectrics. *Adv. Phys.* **2018**, *67*, 69–147. doi:10.1080/00018732.2018.1551715. [1337](#)
75. Li, S.; Li, X.; Ren, Z.; Zhang, Q. Recent progress towards high performance of tin chalcogenide thermoelectric materials. *J. Mater. Chem. A* **2018**, *6*, 2432–2448. doi:10.1039/C7TA09941J. [1338](#)
76. Li, X.; Li, Z.; Chen, C.; Ren, Z.; Wang, C.; Liu, X.; Zhang, Q.; Chen, S. CALPHAD as a powerful technique for design and fabrication of thermoelectric materials as a powerful technique for design and fabrication of thermoelectric materials. *J. Mater. Chem. A* **2021**, *9*, 6634–6649. doi:10.1039/D0TA12620A. [1339](#)
77. Ren, W.; Shi, X.; Wang, Z.; Ren, Z. Crystallographic design for half-Heuslers with low lattice thermal conductivity. *Mater. Today Phys.* **2022**, *25*, 100704. doi:10.1016/j.mtphys.2022.100704. [1340](#)
78. Jia, N.; Cao, J.; Tan, X.Y.; Dong, J.; Liu, H.; Tan, C.K.I.; Xu, J.; Yan, Q.; Loh, X.J.; Suwardi, A. Thermoelectric materials and transport physics. *Mater. Today Phys.* **2021**, *21*, 100519. doi:10.1016/j.mtphys.2021.100519. [1341](#)
79. Basu, R.; Singh, A. High temperature Si-Ge alloy towards thermoelectric applications: A comprehensive review. *Mater. Today Phys.* **2021**, *21*, 100468. [1342](#)
80. New trends, strategies and opportunities in thermoelectric materials: A perspective. *Mater. Today Phys.* **2017**, *1*, 50–60. doi:10.1016/j.mtphys.2017.06.001. [1343](#)
81. Recent progress and future challenges on thermoelectric Zintl materials. *Mater. Today Phys.* **2017**, *1*, 74–95. doi:10.1016/j.mtphys.2017.06.003. [1344](#)
82. Shan, J.; Dejene, F.K.; Leutenantsmeyer, J.C.; Flipse, J.; Münzenberg, M.; van Wees, B.J. Comparison of the magneto-Peltier and magneto-Seebeck effects in magnetic tunnel junctions. *Phys. Rev. B* **2015**, *92*, 020414. doi:10.1103/PhysRevB.92.020414. [1345](#)
83. Liebing, N.; Serrano-Guisan, S.; Krzysteczko, P.; Rott, K.; Reiss, G.; Langer, J.; Ocker, B.; Schumacher, H.W. Tunneling magneto thermocurrent in CoFeB/MgO/CoFeB based magnetic tunnel junctions. *Appl. Phys. Lett.* **2013**, *102*, 242413. doi:10.1063/1.4811737. [1346](#)
84. Liebing, N.; Serrano-Guisan, S.; Rott, K.; Reiss, G.; Langer, J.; Ocker, B.; Schumacher, H.W. Determination of spin-dependent Seebeck coefficients of CoFeB/MgO/CoFeB magnetic tunnel junction nanopillars. *J. Appl. Phys.* **2012**, *111*. doi:10.1063/1.3679769. [1347](#)
85. Böhnert, T.; Dutra, R.; Sommer, R.L.; Paz, E.; Serrano-Guisan, S.; Ferreira, R.; Freitas, P.P. Influence of the thermal interface resistance on the thermovoltage of a magnetic tunnel junction. *Phys. Rev. B* **2017**, *95*, 104441. doi:10.1103/PhysRevB.95.104441. [1348](#)
86. Walter, M.; Walowski, J.; Zbarsky, V.; Münzenberg, M.; Schäfers, M.; Ebke, D.; Reiss, G.; Thomas, A.; Peretzki, P.; Seibt, M.; et al. Seebeck effect in magnetic tunnel junctions. *Nature Materials* **2011**, *10*, 742–746. doi:10.1038/nmat3076. [1349](#)
87. Boehnke, A.; Walter, M.; Roschewsky, N.; Eggebrecht, T.; Drewello, V.; Rott, K.; Münzenberg, M.; Thomas, A.; Reiss, G. Time-resolved measurement of the tunnel magneto-Seebeck effect in a single magnetic tunnel junction. *Review of Scientific Instruments* **2013**, *84*. doi:10.1063/1.4811130. [1350](#)
88. Huebner, T.; Boehnke, A.; Martens, U.; Thomas, A.; Schmalhorst, J.M.; Reiss, G.; Münzenberg, M.; Kuschel, T. Comparison of laser-induced and intrinsic tunnel magneto-Seebeck effect in CoFeB/MgAl₂O₄ and CoFeB/MgO magnetic tunnel junctions. *Phys. Rev. B* **2016**, *93*, 224433. doi:10.1103/PhysRevB.93.224433. [1351](#)
89. Lin, W.; Hehn, M.; Chaput, L.; Negulescu, B.; Andrieu, S.; Montaigne, F.; Mangin, S. Giant spin-dependent thermoelectric effect in magnetic tunnel junctions. *Nat. Commun.* **2012**, *3*, 744. doi:10.1038/ncomms1748. [1352](#)
90. Liebing, N.; Serrano-Guisan, S.; Rott, K.; Reiss, G.; Langer, J.; Ocker, B.; Schumacher, H.W. Tunneling magnetothermopower in magnetic tunnel junction nanopillars. *Phys. Rev. Lett.* **2011**, *107*, 177201. doi:10.1103/PhysRevLett.107.177201. [1353](#)
91. Böhnert, T.; Paz, E.; Ferreira, R.; Freitas, P.P. Magnetic tunnel junction thermocouple for thermoelectric power harvesting. *Phys. Lett. A* **2018**, *382*, 1437–1440. doi:10.1016/j.physleta.2018.02.029. [1354](#)
92. Ellsworth, D.; Lu, L.; Lan, J.; Chang, H.; Li, P.; Wang, Z.; Hu, J.; Johnson, B.; Bian, Y.; Xiao, J.; et al. Photo-spin-voltaic effect. *Nat. Phys.* **2016**, *12*, 861–866. doi:10.1038/nphys3738. [1355](#)
93. Weiler, M.; Huebl, H.; Goerg, F.S.; Czeschka, F.D.; Gross, R.; Goennenwein, S.T.B. Spin pumping with coherent elastic waves. *Phys. Rev. Lett.* **2012**, *108*, 176601. doi:10.1103/PhysRevLett.108.176601. [1356](#)
94. Xu, M.; Puebla, J.; Auvray, F.; Rana, B.; Kondou, K.; Otani, Y. Inverse Edelstein effect induced by magnon-phonon coupling. *Phys. Rev. B* **2018**, *97*, 180301. doi:10.1103/PhysRevB.97.180301. [1357](#)
95. Gui, Y.S.; Xiao, Y.; Bai, L.H.; Hemour, S.; Zhao, Y.P.; Houssameddine, D.; Wu, K.; Guo, H.; Hu, C.M. High sensitivity microwave detection using a magnetic tunnel junction in the absence of an external applied magnetic field. *Appl. Phys. Lett.* **2015**, *106*, 152403. doi:10.1063/1.4918677. [1358](#)
96. Kaiju, H.; Fujita, S.; Morozumi, T.; Shiiki, K. Magnetocapacitance effect of spin tunneling junctions. *J. Appl. Phys.* **2002**, *91*, 7430–7432. doi:10.1063/1.1451754. [1359](#)
97. Kaiju, H.; Takei, M.; Misawa, T.; Nagahama, T.; Nishii, J.; Xiao, G. Large magnetocapacitance effect in magnetic tunnel junctions based on Debye-Fröhlich model. *Appl. Phys. Lett.* **2015**, *107*, 132405. doi:10.1063/1.4932093. [1360](#)
98. Kaiju, H.; Misawa, T.; Nagahama, T.; Komine, T.; Kitakami, O.; Fujioka, M.; Nishii, J.; Xiao, G. Robustness of voltage-induced magnetocapacitance. *Sci. Rep.* **2018**, *8*, 14709. doi:10.1038/s41598-018-33065-y. [1361](#)

99. Kaiju, H.; Nagahama, T.; Sasaki, S.; Shimada, T.; Kitakami, O.; Misawa, T.; Fujioka, M.; Nishii, J.; Xiao, G. Inverse tunnel magnetocapacitance in Fe/Al-oxide/Fe₃O₄. *Sci. Rep.* **2017**, *7*, 2682. doi:10.1038/s41598-017-02361-4. 1393
1394
100. Lee, T.H.; Chen, C.D. Probing spin accumulation induced magnetocapacitance in a single electron transistor. *Sci. Rep.* **2015**, *5*, 13704. doi:10.1038/srep13704. 1395
1396
101. Sato, K.; Sukegawa, H.; Ogata, K.; Xiao, G.; Kaiju, H. Large magnetocapacitance beyond 420% in epitaxial magnetic tunnel junctions with an MgAl₂O₄ barrier. *Sci. Rep.* **2022**, *12*, 7190. doi:10.1038/s41598-022-11545-6. 1397
1398
102. Hai, P.N.; Ohya, S.; Tanaka, M.; Barnes, S.E.; Maekawa, S. Electromotive force and huge magnetoresistance in magnetic tunnel junctions. *Nature* **2009**, *458*, 489–492. doi:10.1038/nature07879. 1399
1400
103. Grieder, P.K.F. *Cosmic Rays at Earth*; Elsevier Science, 2001. ISBN: 9780444507105. 1401
104. https://radhome.gsfc.nasa.gov/radhome/nat_space_rad_tech.htm. 1402
105. Baumann, R.; Kruckmeyer, K. *Radiation Handbook for Electronics: A compendium of radiation effects topics for space, industrial and terrestrial applications*; Texas Instruments, 2020. 1403
1404
106. Haynes, W.M., Ed. *CRC Handbook of Chemistry and Physics*, 92nd ed.; CRC Press: Boca Raton, 2011. 1405
107. Vollmer, M. Physics of the microwave oven. *Physics Education* **2004**, *39*, 74–81. doi:10.1088/0031-9120/39/1/006. 1406
108. https://en.wikipedia.org/wiki/GSM_frequency_bands. 1407
109. https://en.wikipedia.org/wiki/Cellular_frequencies_in_the_United_States. 1408
110. <https://en.wikipedia.org/wiki/5G>. 1409
111. An, S.; Shang, W.; Jiang, M.; Luo, Y.; Fu, B.; Song, C.; Tao, P.; Deng, T. Human hand as a powerless and multiplexed infrared light source for information decryption and complex signal generation. *Proceedings of the National Academy of Sciences* **2021**, *118*, e2021077118. doi:10.1073/pnas.2021077118. 1410
1411
112. Elghafari, M.; McClure, S. Radiation effects assessment of MRAM devices. Technical report, Jet Propulsion Laboratory, 2008. 1412
113. Zhao, G.Y.; Deng, H.; Tyree, N.; Guy, M.; Lisfi, A.; Peng, Q.; Yan, J.A.; Wang, C.; Lan, Y. Recent Progress on Irradiation-Induced Defect Engineering of Two-Dimensional 2H-MoS₂ Few Layers. *Appl. Sci.* **2019**, *9*, 678–678. doi:10.3390/app9040678. 1414
1415
114. Pomeroy, J.; Grube, H.; Perrella, A.; Gillaspy, J. STM and transport measurements of highly charged ion modified materials. *Nucl. Instrum. Meth. B* **2007**, *258*, 189–193. doi:10.1016/j.nimb.2006.12.193. 1416
1417
115. Kobayashi, D.; Kakehashi, Y.; Hirose, K.; Onoda, S.; Makino, T.; Ohshima, T.; Ikeda, S.; Yamanouchi, M.; Sato, H.; Enobio, E.C.; et al. Influence of heavy ion irradiation on perpendicular-anisotropy CoFeB-MgO magnetic tunnel junctions. *IEEE Trans. Nucl. Sci.* **2014**, *61*, 1710–1716. doi:10.1109/TNS.2014.2304738. 1418
1419
1420
116. Cost, J.; Brown, R.; Giorgi, A.; Stanley, J. Effects of neutron irradiation on Nd-Fe-B magnetic properties. *IEEE Trans. Magnet.* **1988**, *24*, 2016–2019. doi:10.1109/20.3393. 1421
1422
117. Liu, B.; Tahmasebi, T.; Ong, K.; Teo, H.; Mo, Z.; Lam, J.; Tan, P.K.; Zhao, Y.; Dong, Z.; Houssameddine, D.; et al. Electron radiation-induced material diffusion and nanocrystallization in nanostructured amorphous CoFeB thin film. *Acta Mater.* **2018**, *161*, 221–236. doi:10.1016/j.actamat.2018.05.060. 1423
1424
1425
118. Beach, L.A.; Theus, R.B.; Faust, W.R. Penetration of gamma radiation through iron. *Phys. Rev.* **1953**, *92*, 355–355. doi:10.1103/PhysRev.92.355. 1426
1427
119. Shkapa, V.M.; Shalaev, A.M.; Polotnjuk, V.V.; Likhtorovich, S.P.; Nemoshkalenko, V.V.; Kotov, V.V. Positron, Mössbauer and NMR studies of γ -irradiated FeCoB metallic glasses. *J. Non. Cryst. Solids* **1993**, *155*, 90–94. doi:10.1016/0022-3093(93)90475-D. 1428
1429
120. Hughes, H.; Bussmann, K.; McMarr, P.J.; Cheng, S.; Shull, R.; Chen, A.P.; Schafer, S.; Mewes, T.; Ong, A.; Chen, E.; et al. Radiation studies of spin-transfer torque materials and devices. *IEEE Trans. Nucl. Sci.* **2012**, *59*, 3027–3033. doi:10.1109/TNS.2012.2223487. 1430
1431
121. Wang, B.; Wang, Z.; Cao, K.; Bi, X.; Zhao, Y.; Zhang, Y.; Zhao, W. Effects of gamma irradiation on magnetic properties of double-interface CoFeB/MgO multilayers. *IEEE Trans. Nucl. Sci.* **2019**, *66*, 77–81. doi:10.1109/TNS.2018.2885338. 1432
1433
122. Arshak, K.; Morris, D.; Kaneshwaran, K.; Korostynska, O.; Arshak, A. Portable real-time gamma radiation dosimetry system using MgO and CeO₂ thick film capacitors. Proceedings of 1st International Conference on Sensing Technology; Gupta, G.S.; Mukhopadhyay, S.C.; Messom, C.H., Eds.; , 2005; pp. 137–142. 1434
1435
1436
123. Hands, A.D.P.; Ryden, K.A.; Meredith, N.P.; Glauert, S.A.; Horne, R.B. Radiation Effects on Satellites During Extreme Space Weather Events. *Space Weather* **2018**, *16*, 1216–1226. doi:10.1029/2018SW001913. 1437
1438
124. Taurian, O.E.; Springborg, M.; Christensen, N.E. Self-consistent electronic structures of MgO and SrO. *Solid State Commun.* **1985**, *55*, 351–355. doi:10.1016/0038-1098(85)90622-2. 1439
1440
125. Suzuki, R.; Tadano, Y.; Tanaka, M.; Ohya, S. Large tunnel magnetoresistance in a fully epitaxial double-barrier magnetic tunnel junction of Fe/MgO/Fe/ γ -Al₂O₃/Nb-doped SrTiO₃. *AIP Adv.* **2020**, *10*, 085115. doi:10.1063/5.0002536. 1441
1442
126. Gayen, A.; Prasad, G.K.; Mallik, S.; Bedanta, S.; Perumal, A. Effects of composition, thickness and temperature on the magnetic properties of amorphous CoFeB thin films. *J. Alloys Compd.* **2017**, *694*, 823–832. doi:10.1016/j.jallcom.2016.10.066. 1443
1444
127. Köster, U.; Herold, U. Crystallization of amorphous Fe₈₀B₂₀. *Scr. Metall.* **1978**, *12*, 75–77. doi:10.1016/0378-4363(88)90252-5. 1445
128. Roy, R.; Majumdar, A. Thermomagnetic and transport properties of metglas 2605 SC and 2605. *J. Magn. Magn. Mater.* **1981**, *25*, 83–89. doi:10.1016/0304-8853(81)90150-5. 1446
1447
129. Srivastava, S.; Chen, A.; Dutta, T.; Ramaswamy, R.; Son, J.; Saifullah, M.; Yamane, K.; Lee, K.; Teo, K.L.; Feng, Y.P.; et al. Effect of (Co_xFe_{1-x})₈₀B₂₀ composition on the magnetic properties of the free layer in double-barrier magnetic tunnel junctions. *Phys. Rev. Appl.* **2018**, *10*, 024031. doi:10.1103/PhysRevApplied.10.024031. 1448
1449
1450
130. Binder, D.; Smith, E.; Holman, A. Satellite anomalies from galactic cosmic rays. *IEEE Trans. Nucl. Sci.* **1975**, *22*, 2675–2680. 1451

131. Ziegler, J.; Nelson, M.; Shell, J.; Peterson, R.; Gelderloos, C.; Muhlfeld, H.; Montrose, C. Cosmic ray soft error rates of 16-Mb DRAM memory chips. *IEEE J. Solid-State Circuits* **1998**, *33*, 246–252. doi:10.1109/4.658626. 1452
1453
132. MacLaren, J.M.; Zhang, X.G.; Butler, W.H. Validity of the Julliere model of spin-dependent tunneling. *Phys. Rev. B* **1997**, *56*, 11827–11832. doi:10.1103/PhysRevB.56.11827. 1454
1455
133. Soulé, R.J.; Byers, J.M.; Osofsky, M.S.; Nadgorny, B.; Ambrose, T.; Cheng, S.F.; Broussard, P.R.; Tanaka, C.T.; Nowak, J.; Moodera, J.S.; et al. Measuring the spin polarization of a metal with a superconducting point contact. *Science* **1998**, *282*, 85–88. 1456
1457
1458
134. Butler, W.H.; Zhang, X.G.; Schulthess, T.C.; MacLaren, J.M. Spin-dependent tunneling conductance of Fe|MgO|Fe sandwiches. *Phys. Rev. B* **2001**, *63*, 054416. doi:10.1103/PhysRevB.63.054416. 1459
1460
135. Mathon, J.; Umerski, A. Theory of tunneling magnetoresistance of an epitaxial Fe/MgO/Fe(001) junction. *Phys. Rev. B* **2001**, *63*, 220403. doi:10.1103/PhysRevB.63.220403. 1461
1462
136. Michelena, M.; Arruego, I.; Oter, J.; Guerrero, H. COTS-based wireless magnetic sensor for small satellites. *IEEE Trans. Aerosp. Electron. Syst.* **2010**, *46*, 542–557. doi:10.1109/TAES.2010.5461640. 1463
1464
137. Stutzke, N.A.; Russek, S.E.; Pappas, D.P.; Tondra, M. Low-frequency noise measurements on commercial magnetoresistive magnetic field sensors. *J. Appl. Phys.* **2005**, *97*, 10Q107. doi:10.1063/1.1861375. 1465
1466
138. Heidecker, J.; Allen, G.; Sheldon, D. Single event latchup (SEL) and total ionizing dose (TID) of a 1 Mbit magnetoresistive random access memory (MRAM). Radiation Effects Data Workshop (REDW), 2010, p. 4. doi:10.1109/REDW.2010.5619499. 1467
1468
139. Hass, K.J.; Donohoe, G.W.; Hong, Y.K.; Choi, B.C. Magnetic flip flops for space applications. *IEEE Trans. Magn.* **2006**, *42*, 2751. 1469
doi:10.1109/TMAG.2006.879738.
1470
140. Lu, J.; Poon, S.J.; Wolf, S.A.; Weaver, B.D.; McMarr, P.J.; Hughes, H.; Chen, E. Radiation effects on the magnetism and the spin dependent transport in magnetic materials and nanostructures for spintronic applications. *J. Mater. Res.* **2015**, *30*, 1430–1439. 1471
1472
1473
141. Sze, K.; Musazi, K.; Farrell, G.; Budhani, R.; Lan, Y. Electron Irradiation Tolerance of Molybdenum Disulfide Two-dimensional Nanolayers Investigated from Electron Diffraction. *Microsc. Microanal.* **2022**, *28*, 2366–2367. doi:10.1017/S1431927622009084. 1474
1475
142. Pomeroy, J.; Lake, R.; Sosolik, C. Highly charged ion interactions with thin insulating films. *Nucl. Instrum. Meth. B* **2011**, *269*, 1238–1242. doi:10.1016/j.nimb.2010.11.006. 1476
1477
143. Conraux, Y.; Nozières, J.P.; Da Costa, V.; Toulemonde, M.; Ounadjela, K. Effects of swift heavy ion bombardment on magnetic tunnel junction functional properties. *J. Appl. Phys.* **2003**, *93*, 7301–7303. doi:10.1063/1.1558659. 1478
1479
144. Nowak, E.R.; Weissman, M.B.; Parkin, S.S.P. Electrical noise in hysteretic ferromagnet–insulator–ferromagnet tunnel junctions. *Appl. Phys. Lett.* **1999**, *74*, 600–602. doi:10.1063/1.123158. 1480
1481
145. Moodera, J.S.; Nassar, J.; Mathon, G. Spin-tunneling in ferromagnetic junctions. *Annu. Rev. Mater. Sci.* **1999**, *29*, 381–432. 1482
doi:10.1146/annurev.matsci.29.1.381.
1483
146. Gordon, D.; Sery, R. Effects of charged particles and neutrons on magnetic materials. *IEEE Trans. Commun. Electr.* **1964**, *83*, 357–361. doi:10.1109/TCOME.1964.6541237. 1484
1485
147. Groult, D.; Hervieu, M.; Nguyen, N.; Raveau, B.; Fuchs, G.; Balanzat, E. Amorphization induced by energetic heavy ion bombardment in hexagonal ferrite BaFe₁₂O₁₉. *Radiat. Eff.* **1985**, *90*, 191–204. doi:10.1080/00337578508222531. 1486
1487
148. Chukalkin, Y.G.; Petrov, V.V.; Goshchitskii, B.N. Radiation effects in hexagonal ferrite BaFe₁₂O₁₉. *Phys. Status Solidi A* **1981**, *67*, 421–426. doi:10.1002/pssa.2210670209. 1488
1489
149. Ofan, A.; Gaathon, O.; Zhang, L.; Evans-Lutterodt, K.; Bakhrus, S.; Bakhrus, H.; Zhu, Y.; Welch, D.; Osgood, R.M. Twinning and dislocation pileups in heavily implanted LiNbO₃. *Phys. Rev. B* **2011**, *83*, 064104. doi:10.1103/PhysRevB.83.064104. 1490
1491
150. Huang, H.C.; Dadap, J.I.; Gaathon, O.; Herman, I.P.; Osgood, R.M.; Bakhrus, S.; Bakhrus, H. A micro-Raman spectroscopic investigation of He⁺-irradiation damage in LiNbO₃. *Opt. Mater. Express* **2013**, *3*, 126–142. doi:10.1364/OME.3.000126. 1492
1493
151. Kobayashi, D.; Hirose, K.; Makino, T.; Onoda, S.; Ohshima, T.; Ikeda, S.; Sato, H.; Enobio, E.C.I.; Endoh, T.; Ohno, H. Soft errors in 10-nm-scale magnetic tunnel junctions exposed to high-energy heavy-ion radiation. *Jpn. J. Appl. Phys.* **2017**, *56*, 0802B4–1–0802B4–10. doi:10.7567/JJAP.56.0802B4. 1494
1495
1496
152. Ren, F.; Jander, A.; Dhagat, P.; Nordman, C. Radiation tolerance of magnetic tunnel junctions with MgO tunnel barriers. *IEEE Trans. Nucl. Sci.* **2012**, *59*, 3034–3038. doi:10.1109/TNS.2012.2224375. 1497
1498
153. Ono, K.; Ohshima, N.; Goto, K.; Yamamoto, H.; Morita, T.; Kinoshita, K.; Ishijima, T.; Toyoda, H. Effect of O-ion beam irradiation during RF-magnetron sputtering on characteristics of CoFeB-MgO magnetic tunnel junctions. *Jpn. J. Appl. Phys.* **2011**, *50*, 023001. 1499
1500
1501
154. Snoeck, E.; Baules, P.; BenAssayag, G.; Tiusan, C.; Greullet, F.; Hehn, M.; Schuhl, A. Modulation of interlayer exchange coupling by ion irradiation in magnetic tunnel junctions. *J. Phys.: Condens. Matter.* **2008**, *20*, 055219. doi:10.1088/0953-8984/20/5/055219. 1502
1503
155. Martinelli, A.; Tarantini, C.; Lehmann, E.; Manfrinetti, P.; Palenzona, A.; Pallegatti, I.; Putti, M.; Ferdeghini, C. Direct TEM observation of nanometric-sized defects in neutron-irradiated MgB₂ bulk and their effect on pinning mechanisms. *Supercond. Sci. Tech.* **2008**, *21*, 012001. doi:10.1088/0953-2048/21/01/012001. 1504
1505
1506
156. Singh, B.N.; Horsewell, A.; Toft, P.; Edwards, D.J. Temperature and dose dependencies of microstructure and hardness of neutron irradiated OFHC copper. *J. Nucl. Mater.* **1995**, *224*, 131–140. doi:10.1016/0022-3115(95)00054-2. 1507
1508
157. Škorvánek, I.; Idzikowski, B.; Zentko, A.; Mosiniewicz-Szablewska, E. Influence of neutron irradiation on the magnetic properties of FeNiCrMoSiB amorphous alloys. *Phys. Status Solidi A* **1988**, *108*, 747–751. doi:10.1002/pssa.2211080232. 1509
1510

158. Nikiforov, S.V.; Kortov, V.S.; Petrov, M.O. Luminescent and dosimetric properties of ultrafine magnesium oxide ceramics after high dose irradiation. *Radiat. Meas.* **2016**, *90*, 252–256. doi:10.1016/j.radmeas.2015.12.018. 1512
159. Sibley, W.A.; Kolopus, J.L.; Mallard, W.C. A study of the effect of deformation on the ESR, luminescence, and absorption of MgO single crystals. *Phys. Status Solidi B* **1969**, *31*, 223 – 231. doi:10.1002/pssb.19690310126. 1513
- 1514
160. Abramishvili, M.G.; Altukhov, V.I.; Kalabegishvili, T.L.; Kvachadze, V.G. Low-temperature heat conduction of γ -irradiated MgO crystals. *Phys. Status Solidi B* **1981**, *104*, 49 – 55. doi:10.1002/pssb.2221040104. 1515
- 1516
161. Kvatchadze, V.; Dekanozishvili, G.; Kalabegishvili, T.; Gritsyna, V.; Tavkhelidze, V. Dosimetric properties of magnesium oxide crystals. *J. Mater. Sci. Eng. A* **2011**, *1*, 872 – 875. 1517
- 1518
162. Kiesh, Y.; Kristianpoller, N.; Chen, R. Vacuum ultra-violet induced thermoluminescence in γ -irradiated and non-irradiated MgO powder. *Philos. Mag.* **1977**, *35*, 653–661. doi:10.1080/14786437708235997. 1519
- 1520
163. Soliman, C. Thermoluminescence behavior of magnesium oxide exposed to gamma and ultraviolet radiations. *Radiat. Eff. Defects Solids* **2009**, *164*, 257–265. doi:10.1080/10420150802349518. 1521
- 1522
164. Nguyen, H.; Persson, A.; Thornell, G. Material- and fabrication-governed performance of a tunnelling magnetometer. The 5th International Workshop on Advanced Materials Science and Nanotechnology (IWAMSN2010); , 2010. 1523
- 1524
165. Persson, A.; Thornell, G.; Nguyen, H. Radiation tolerance of a spin-dependent tunnelling magnetometer for space applications. *Meas. Sci. Technol.* **2011**, *22*, 045204. doi:10.1088/0957-0233/22/4/045204. 1525
- 1526
166. Sinclair, R.; Beech, R. High speed, radiation hard MRAM buffer. The 2002 Non-Volatile Memory Technology Symposium; , 2002. 1527
167. Kang, W.; Zhao, W.; Deng, E.; Klein, J.O.; Cheng, Y.; Ravelosona, D.; Zhang, Y.; Chappert, C. A radiation hardened hybrid spintronic/CMOS nonvolatile unit using magnetic tunnel junctions. *J. Phys. D: Appl. Phys.* **2014**, *47*, 405003. doi:10.1088/0022-3727/47/40/405003. 1528
- 1529
168. Arshak, K.; Kaneswaran, K.; Korostynska, O.; Morris, D.; Arshak, A. Wireless real-time gamma radiation dosimetry system using MgO and CeO₂ thick film capacitors. Proceedings of the 2006 IEEE Sensors Applications Symposium; IEEE Instrumentation and Measurement Society: Houston, Texas, USA, 2006; pp. 60 – 65. doi:10.1109/SAS.2006.1634237. 1530
- 1531
- 1532
- 1533
169. Steinike, U.; Barsova, L.I.; Jurik, T.K.; Hennig, H.P. Effect of γ -radiation on mechanically processed MgO powder (compressive and shear stress). *Kristall und Technik* **1981**, *16*, 971 – 976. doi:10.1002/crat.19810160818. 1534
- 1535
170. Clement, S.; Hodgson, E.R. Correlation between Fe, Cr, and the broad red emission band in γ -ray-irradiated MgO. *Phys. Rev. B* **1984**, *30*, 4684 – 4688. doi:10.1103/PhysRevB.30.4684. 1536
- 1537
171. Lynch, G.F. Ionic and Gamma-ray Induced Photoconductivity of MgO. *Can. J. Phys.* **1975**, *53*, 210 – 218. doi:10.1139/p75-032. 1538
172. Wang, Z.; Saito, M.; McKenna, K.P.; Fukami, S.; Sato, H.; Ikeda, S.; Ohno, H.; Ikuhara, Y. Atomic-scale structure and local chemistry of CoFeB-MgO magnetic tunnel junctions. *Nano Lett.* **2016**, *16*, 1530 – 1536. doi:10.1021/acs.nanolett.5b03627. 1539
- 1540
173. Piñera, I.; Cruz, C.M.; Leyva, A.; Abreu, Y.; Cabal, A.E.; Espen, P.V.; Remortel, N.V. Improved calculation of displacements per atom cross section in solids by gamma and electron irradiation. *Nucl. Instrum. Meth. B* **2014**, *339*, 1 – 7. doi:10.1016/j.nimb.2014.08.020. 1541
- 1542
- 1543
174. Smith, R.A.; Sanford, R.; Warnock, F.E. Radiation effects on an all thin film amorphous memory device. *Journal of Non-Crystalline Solids* **1972**, *8-10*, 862 – 867. doi:10.1016/0022-3093(72)90239-6. 1544
- 1545
175. Młyńczak, E.; Freindl, K.; Spiridis, N.; Korecki, J. Epitaxial MgO/Fe(001) and Fe/MgO(001): Structures of the interfaces. *J. Appl. Phys.* **2013**, *113*, 024320. doi:10.1063/1.4775707. 1546
- 1547
176. Jamal, M.S.; Gupta, P.; Sergeev, I.; Leupold, O.; Kumar, D. Interface-resolved study of magnetism in MgO/FeCoB/MgO trilayers using x-ray standing wave techniques. *Phys. Rev. B* **2023**, *107*, 075416. doi:10.1103/PhysRevB.107.075416. 1548
- 1549
177. Ueda, S.; Mizuguchi, M.; Tsujikawa, M.; Shirai, M. Electronic structures of MgO/Fe interfaces with perpendicular magnetization revealed by hard X-ray photoemission with an applied magnetic field. *Science and Technology of Advanced Materials* **2019**, *20*, 796 – 804. doi:10.1080/14686996.2019.1633687. 1550
- 1551
- 1552
178. Gerward, L. On the attenuation of X-rays and γ -rays in dilute solutions. *Radiation Physics and Chemistry* **1996**, *48*, 697 – 699. doi:10.1016/S0969-806X(96)00131-4. 1553
- 1554
179. Baur, M.; Uhlmann, N.; Pöschel, T.; Schröter, M. Correction of beam hardening in X-ray radiograms. *Review of Scientific Instruments* **2019**, *90*, 025108. doi:10.1063/1.5080540. 1555
- 1556
180. Daneshvar, H.; Milan, K.G.; Sadr, A.; Sedighy, S.H.; Malekia, S.; Mosayebi, A. Multilayer radiation shield for satellite electronic components protection. *Scientific Reports* **2021**, *11*, 20657. doi:10.1038/s41598-021-99739-2. 1557
- 1558
181. Ikeda, S.; Miura, K.; Yamamoto, H.; Mizunuma, K.; Gan, H.D.; Endo, M.; Kanai, S.; Hayakawa, J.; Matsukura, F.; Ohno, H. A perpendicular-anisotropy CoFeB-MgO magnetic tunnel junction. *Nat. Mater.* **2010**, *9*, 721 – 724. doi:10.1038/nmat2804. 1559
- 1560
182. Zhang, J.; Wang, Y.; Zhang, X.G.; Han, X.F. Inverse and oscillatory magnetoresistance in Fe(001)/MgO/Cr/Fe magnetic tunnel junctions. *Phys. Rev. B* **2010**, *82*, 134449. doi:10.1103/PhysRevB.82.134449. 1561
- 1562
183. Tsypin, S.G.; Kukhtevich, V.I.; Kazansky, Y.A. The penetration of gamma-rays through water, iron, lead, and combinations of iron and lead. *Sov. J. At. Energy* **1956**, *1*, 217 – 220. doi:10.1007/BF01506934. 1563
- 1564
184. Nagahama, T.; Yuasa, S.; Tamura, E.; Suzuki, Y. Spin-dependent tunneling in magnetic tunnel junctions with a layered antiferromagnetic Cr(001) spacer: Role of band structure and interface scattering. *Phys. Rev. Lett.* **2005**, *95*, 086602. doi:10.1103/PhysRevLett.95.086602. 1565
- 1566
- 1567
185. Rotstein, B.H.; Stephenson, N.A.; Vasdev, N.; Liang, S.H. Spirocyclic hypervalent iodine (III)-mediated radiofluorination of non-activated and hindered aromatics. *Nat. Commun.* **2014**, *5*, 1 – 7. doi:10.1038/ncomms5365. 1568
- 1569

186. Oh, S.C.; Park, S.Y.; Manchon, A.; Chshiev, M.; Han, J.H.; Lee, H.W.; Lee, J.E.; Nam, K.T.; Jo, Y.; Kong, Y.C.; et al. Bias-voltage dependence of perpendicular spin-transfer torque in asymmetric MgO-based magnetic tunnel junctions. *Nat. Phys.* **2009**, *5*, 898–902. doi:10.1038/nphys1427. 1570
187. Dhar, A.; DeWerd, L.A.; Stoebe, T.G. Direct-response ultraviolet thermoluminescent dosimeter. *Med. Phys.* **1976**, *3*, 415–417. doi:10.1118/1.594259. 1571
188. Las, W.C.; Stoebe, T.G. Thermoluminescent mechanisms involving transition metal ion impurities and V-type centres in MgO crystals exposed to ultraviolet radiation. *J. Mater. Sci.* **1982**, *17*, 2585–2593. doi:10.1007/BF00543891. 1572
189. Duley, W.W.; Rosatzin, M. The orange luminescence band in MgO crystals. *J. Phys. Chem. Solids* **1985**, *46*, 165–170. doi:10.1016/0022-3697(85)90029-0. 1573
190. Shen, W.; Mazumdar, D.; Zou, X.; Liu, X.; Schrag, B.D.; Xiao, G. Effect of film roughness in MgO-based magnetic tunnel junctions. *Appl. Phys. Lett.* **2006**, *88*, 182508. doi:10.1063/1.2201547. 1574
191. Wang, W.G.; Ni, C.; Rumaiz, A.; Wang, Y.; Fan, X.; Moriyama, T.; Cao, R.; Wen, Q.Y.; Zhang, H.W.; Xiao, J.Q. Real-time evolution of tunneling magnetoresistance during annealing in CoFeB-MgO-CoFeB magnetic tunnel junctions. *Appl. Phys. Lett.* **2008**, *92*, 152501. doi:10.1063/1.2903147. 1575
192. Liu, X.; Mazumdar, D.; Shen, W.; Schrag, B.D.; Xiao, G. Thermal stability of magnetic tunneling junctions with MgO barriers for high temperature spintronics. *Appl. Phys. Lett.* **2006**, *89*, 023504. doi:10.1063/1.2219997. 1576
193. Xu, X.; Mukaiyama, K.; Kasai, S.; Ohkubo, T.; Hono, K. Impact of boron diffusion at MgO grain boundaries on magneto-transport properties of MgO/CoFeB/W magnetic tunnel junctions. *Acta Materialia* **2018**, *161*, 360–366. doi:10.1016/j.actamat.2018.09.028. 1577
194. Bai, Z.; Shen, L.; Wu, Q.; Zeng, M.; Wang, J.S.; Han, G.; Feng, Y.P. Boron diffusion induced symmetry reduction and scattering in CoFeB/MgO/CoFeB magnetic tunnel junctions. *Physical Review B* **2013**, *87*, 014114. doi:10.1103/PhysRevB.87.014114. 1578
195. Yoshikawa, N. Fundamentals and Applications of Microwave Heating of Metals. *J. Microw. Power Electromagn. Energy* **2010**, *44*, 4–13. doi:10.1080/08327823.2010.11689772. 1579
196. Cao, Z.; Yoshikawa, N.; Taniguchi, S. Microwave heating behavior of nanocrystalline Au thin films in single-mode cavity. *J. Mater. Res.* **2009**, *24*, 268–273. doi:10.1557/JMR.2009.0030. 1580

Short Biography of Authors



Dereje Seifu Dr. Dereje Seifu is a professor of physics at Morgan State University. He received his Ph. D. degree from the University of Cincinnati in 1994, an MS from both the University of Cincinnati and Addis Ababa University, a certificate from ICTP in Trieste, Italy, and a BS from Addis Ababa University. Dr. Seifu's current research focuses on magnetostrictive materials, tunneling magneto-resistance devices, and 2-D materials. 1591



Qing Peng Dr. Qing Peng is an Associate Professor and K. A. CARE Fellow in the Department of Physics at King Fahd University of Petroleum and Minerals (KFUPM) in Saudi Arabia. Dr. Peng obtained his Ph. D. in Physics from the University of Connecticut in 2005, an MS from the State University of New York at Binghamton, and a BS from Peking University. Dr. Peng's current research in computational materials physics covers various areas such as strain engineering, radiation damage, multiscale modeling, shock physics, ion-batteries, thermoelectrics, and perovskite solar cells. 1601



1606

Jie Hou Mr. Jie Hou is a Ph. D. candidate in the School of Materials Science and Engineering at the Georgia Institute of Technology. He obtained a Bachelor's degree in Optics from Changchun University of Science and Technology, China. Mr. Hou's ongoing research focuses on transmission electron microscopy and fuel cells.



1610

Kit Sze Mr. Kit Sze is a senior student at Morgan State University. He is majoring in Mathematics with a minor in Physics. He currently holds the position of research assistant in the Department of Physics at Morgan State University. He current research focuses on photovoltaic measurements and data analyses. Mr. Sze's research also encompassed computational neuroscience and AI healthcare. He is a member of PI MU EPSILON and holds an Honor Mathematics distinction.



1616

Fei Cao Dr. Fei Gao is a professor at the University of Michigan, holds positions in the Department of Nuclear Engineering and Radiological Sciences as well as the Department of Material Science and Engineering,. Dr. Gao's research is currently focuses on various topics including ion-solid interaction, irradiation damage, detector materials, nanostructure properties, Li⁺ ion batteries, and the advancement of multi-scale material modeling.



1621

Yucheng Lan Dr. Yucheng Lan is a professor of physics at Morgan State University. He obtained his Ph. D. degree from the Institute of Physics at the Chinese Academy of Sciences, master's and bachelor's degrees from Jilin University in China. Dr. Lan's current research focuses on renewable energy, nanomaterials, and sensors, with expertise in X-ray powder diffraction, electron microscopies, and optical spectroscopy.

1622

1623

1624

1625